UNIVERSITA' DEGLI STUDI DI PADOVA

DIPARTIMENTO DI INGEGNERIA INDUSTRIALE

CORSO DI LAUREA MAGISTRALE IN INGEGNERIA DEI MATERIALI

Toughening of RTI CFRP joints using thermoplastic interlayers

Relatore: **Prof. Massimo Guglielmi**

Correlatore: **Prof. Alojz Ivankovic**

Laureando: FILIPPO MOGNON

ANNO ACCADEMICO 2015-2016

Abstract

In this study, the use of thermoplastic interlayers was investigated as a way of increasing the fracture toughness of carbon fiber reinforced epoxy composites. This approach involves the addition of thermoplastic strips during the composite layup process.

In order to investigate this approach, composites with interlayers included would be measured against a control group without an interlayer. Within the group of composite specimen with interlayers, four different materials (PI, PET, PEI and PMMA) and three different interlayer orientations (longitudinal strips, transversal strips and mesh) were trialed. The purpose of this procedure was to assess whether an ideal material and orientation existed.

The testing carried out as part of this study involved three-point bending of composite samples in order to determine the flexural modulus. It also included double cantilever beam testing. This was the main test in this study and it was the method by which fracture toughness was measured. The fracture toughness calculation was based on two commonly used theories: Simple Beam Theory (SBT) and Corrected Beam Theory (CBT).

Results are shown in terms of the fracture toughness' mean value and the resistance curves of the specimens tested. As a conclusion, the best material and the best interlayer orientation were pointed out.

Acknowledgments

I would like to express my heartfelt thanks to all the UCD staff that I have worked with during this amazing experience. Professor Alojz Ivankovic advised me constantly, providing helpful insights and support without whom the project may not have been possible. Deepest thanks also to Clémence Rouge, who was always willing to help me solving every kind of problems with her great knowledge of the subject.

Dr. John Gahan provided great help when manufacturing the composite and carrying out the tests.

Prof. Massimo Guglielmi helped me from Padova during the Erasmus period and after my return, giving me advices and useful recommendations.

I would also like to thank my family: in particular my parents and my girlfriend, who encouraged and supported me during the entire duration of the university and especially during my experience abroad. Grazie!

Contents

List of figures

1. Introduction

1.1. Composite Materials

A composite material is a material made of two or more different phases or materials, obtaining a product with a combination of the characteristics of the individual components. The first composite made by human dates back at least 6000 years: straw and mud were combined in order to form bricks for constructions. Nowadays, the most widely used composite material is concrete, which is produced in approximately 9000 billion tons per year making it the second most used material after water.

Composite materials consist of a matrix phase (continuous) and a reinforcing phase (dispersed). Depending on the nature of the matrix, they are classified as follows [1]:

- Metal Matrix Composites (MMC) have metallic matrix and ceramic or metallic dispersed phase.
- Polymer Matrix Composites (PMC) consist of thermoplastic or thermoset matrix with fibers as reinforcing phase.
- Ceramic Matrix Composites (CMC) are composed of ceramic matrix and another ceramic material as dispersed phase.

Two materials are generally combined in order to obtain a resulting material with the desired properties. In this project, only PMC will be investigated; therefore, the discussion will not include MMC and CMC.

PMC are also known as Fiber Reinforced Polymers (FRP). Depending on the type of fibers that reinforce the polymeric matrix, FRP are divided in [2]:

- GFRP, using Glass fibers; normally polyester or epoxy are used as matrix. GFRP are used for their high strength, electric insulation, stiffness and

resistance to chemical harm [3]. Those composites find applications in electronics, home furniture, aerospace industry, marine industry and medical field.

- AFRP, using Aramid Fibers; these fibers enhance the impact resistance of the matrix and have a low density [4]. Normally epoxy resin is used as matrix. AFRP have applications in helmets and bulletproof vests, boat hulls, aircraft body parts.
- BFRP, using Basalt fiber; these composites are comparable to GFRP, they are stiffer and stronger but heavier than GFRP [5]. BFRP are used in brake systems for their high melting point, in turbine blades and in sport industry (snowboards).
- CFRP, using Carbon fibers; these composite materials will be detailed in the next section.

1.2. CFRP: properties and applications

Carbon fibers date back in 1879, when Thomas Edison used them as a filament for early light bulbs. Their commercial use started from 1950, when rayon and PAN started to be used as precursors. Since the beginning, carbon fibers were known for their interesting properties: they weigh a fraction of the weight of steel and they have higher tensile strength and high modulus.

1.2.1. CFRP market

The high cost of CFRP has limited its diffusion in every-day applications. In the last decade, the need of lightweight transport (that allows the reduction of fuel consumption) caused the increasing demand of CFRP in this field. The overall market

is expected to grow to $35 Billion in 2020, with the price of carbon fibers estimated to fall to 10,5 €/kg [6].

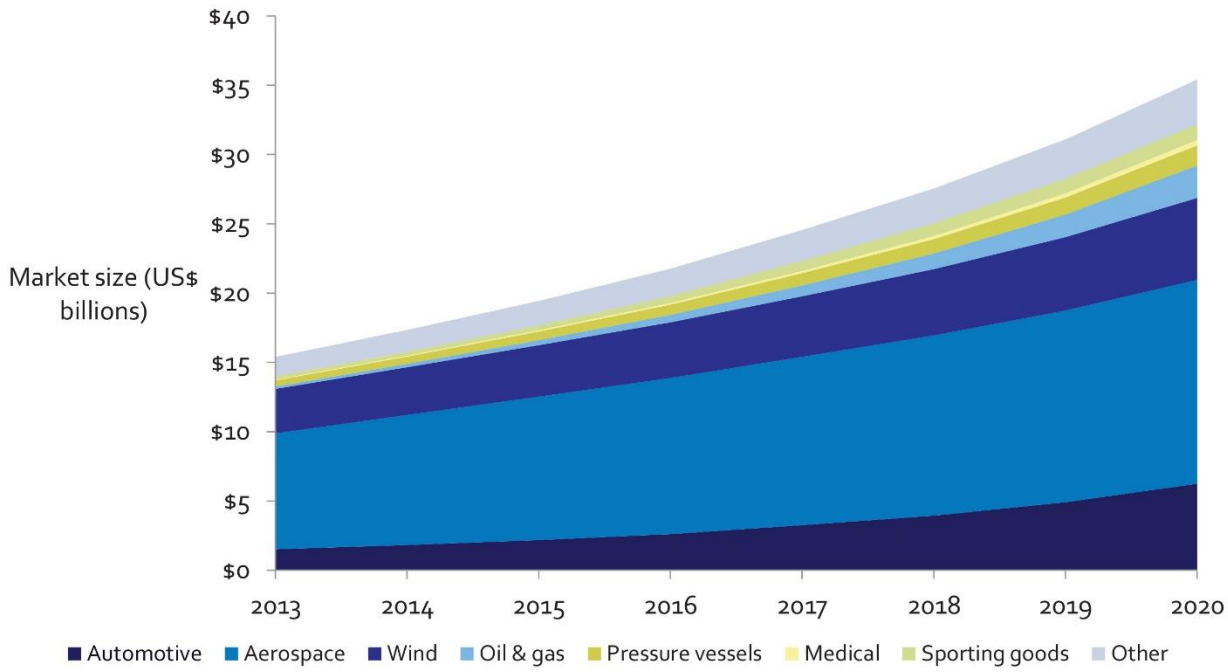

Figure 1. CFRP market 2013 - 2020

Figure 1 points out that more than 50% of the overall CFRP market consists of the sum of automotive and aerospace industries.

Another study estimated that the CFRP demand will reach 212.9 kilo tons in 2022, that compared to the 83.0 kilo tons in 2014 means a growth of 255% in 8 years [7]. The thermoplastic matrix is expected to gain a higher importance because of its high processability and its good recycling properties [7].

1.2.2. Applications in aerospace industry

CFRP are widely used in aerospace industry in particular for their lightness and strength, their durability and their low thermal distortion. There are some disadvantages when employing CFRP in aerospace industry: they often require

reinforcement against impact (achieved with aramid fibers or titanium edges) and the epoxy used for thrust components must resist to very high temperatures.

The first CFRP component that made its appearance in the aerospace industry was the RB211 jet engine developed by Rolls Royce in 1960s. The introduction of this component was unsuccessful because of its poor impact resistance: the jet engine was subject to failure in case of bird strikes.

Since 1980s, composites started to be used for secondary components for wings and tail; each new aircraft had an increasing percentage of composites. With the use of composites replacing aluminium in the airframe, Boeing manages to reach a weight saving of 20% [8]; moreover, the presence of composites allows the reduction of maintenance work thanks to the lower risk of corrosion and fatigue.

Boeing 787 was the first aircraft with more than 50% composite materials, and in particular CFRP. Other composites such as AFRP are used in order to reinforce the edges because of the low impact resistance of carbon laminates.

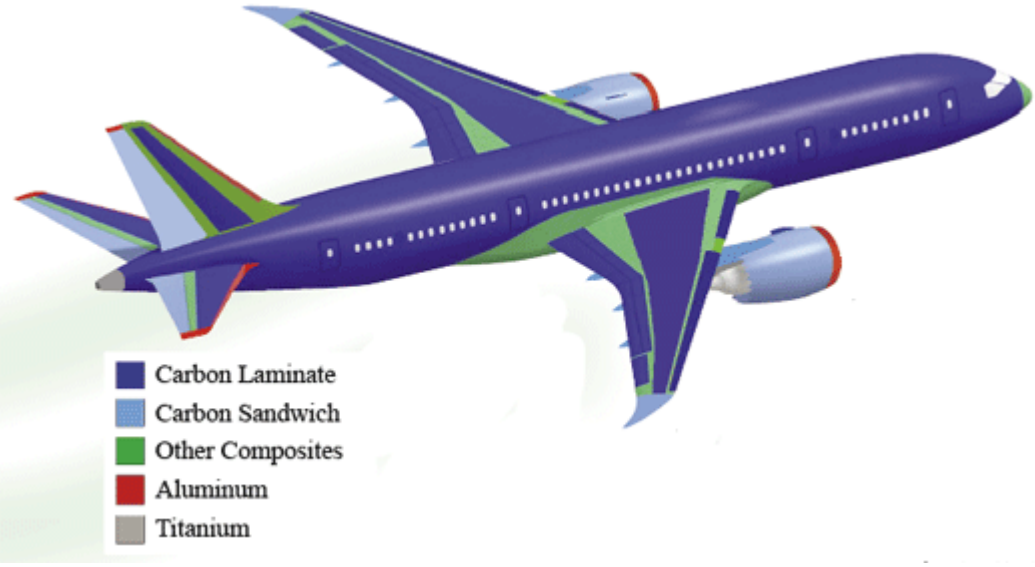

Figure 2. Structure of Boeing 787

Airbus has developed the use of CFRP in their aircrafts, and Airbus A380 is the first airplane to boast a central wing box made of carbon fiber, allowing to save up to one and a half tons compared to the conventional aluminium structure [9].
It is believed that the future of CFRP will involve the use of carbon nanotubes (CNTs), in particular in aerospace industry. The addition of nanotubes will lead to the production of stronger, lighter and more impact-resistant CFRP; CNTs might be involved in the repair of delaminated areas of the composite structure [10] [11].

1.3. Toughening of CFRP

The toughening of composite materials is a subject under rapid development and much effort is employed in this matter. As already pointed out in the introduction, composite materials are normally lighter and stiffer than traditional materials like metals; one of the main problems of the composites is their brittleness in comparison with metals and polymers, thus their application must take into account the probability of failure [12] [13].
The idea at the base of the toughening mechanisms is that the energy required for the crack propagation G_{IC} must be maximized [14]. Toughening processes have been investigated for a wide range of materials, from ceramics to soft composites [15].
There are two main mechanisms of toughening of composites with thermoset matrix, both involving the dispersion of thermoplastic or rubber particles [16]. The first mechanism involves the dispersion of the particles without the creation of a second phase: those particles remain in the matrix and increase the fracture toughness by the increasing of strain to rupture. In the second mechanism, the particles form a multi-phase system and the characteristics of the particles (shape, physical properties, thermal properties) directly influence the fracture toughness.

Kinloch et al. showed that the addition of nano-SiO_2 particles increase the fracture toughness of CFRP composites (manufactured using RTM process) without decreasing their modulus [17].

In the toughening process, the adhesion between the matrix and the fibers and between the particles and the matrix is fundamental: Parker et al. found a lower increment of fracture toughness than expected because the secondary phase did not adhere to the matrix [18].

Further studies involving particle toughening showed that the fracture toughness of a toughened composite with volume of fibers $V_f = 0.20$ is comparable with a non-toughened composite with $V_f = 0.55$ [19].

Carbon nanotubes have received a great deal of attention as reinforcing phase in the last few years because of their high specific strength [20] [21].

Studies including the insertion of a thermoplastic interlayer were carried out in the past: Hojo et al. managed to increase the fracture toughness of CFRP by 3 times with the introduction of an interleaf containing polyamide particles [22]. The interlayer induced the shifting of the crack path increasing the toughness.

A study carried out by Hojo et al. involving the use of an epoxy resin interlayer showed that mode I fracture toughness and mode II fracture toughness are not influenced in the same way. In particular, it was found that the interlayer did not affect G_{IC}, but G_{IIC} was increased by 3 times [23]. Therefore, it would be interesting to evaluate the effect of the interlayer in each mode of fracture. In this project, only mode I is investigated: mode II and mixed modes might be investigated in future works as specified in chapter 6.2.

1.4. Project Objectives

First, many composite plates will be manufactured using Resin Transfer Infusion with the apparatus built by John Mohan in UCD [24].

The main objective of this project is to investigate the behavior of thermoplastic interlayers in the carbon fiber-reinforced plastics produced by RTI using DCB tests. In particular, it is to determine the best material among the four thermoplastics tested; moreover, the best configuration of the interlayer will be established.
In order to calculate the value of the flexural modulus, three-point bending tests will be carried out.

1.5. Project outlines

The project can be divided into the following steps:

- **Manufacturing of the composite plates**
  Several plates are produced using RTI technique, starting from dry fibers and resin. Two plates are manufactured for each curing cycle.
- **Sample preparation and tests**
  Once the plate is cured, it is cut into DCB samples. The specimens are prepared for the test with load blocks and 'Tipp-ex'.
  Two tests are performed: DCB test and three-point bending test. The DCB test determines the value of the fracture toughness of the tested specimen. The three-point bending test measures the value of the flexural modulus and it is carried out with specimens without crack initiator and without thermoplastic interlayer.
- **Data analysis**
  Load-displacement curves and R-curves are analyzed in order to determine the toughness. The values of G_{IC} are compared and the conclusions are outlined.

2. Fracture mechanics

2.1. Chapter overview

In this chapter, the failure analysis approach is outlined. The theory behind the testing methods is investigated for both the three-point bending test and the DCB test.

2.2. Introduction to fracture mechanics

Fracture mechanics is the branch of mechanics that deals with the propagation of cracks in a material. It studies the driving force for the crack growth and the resistance to propagation of the material.

Once man started to build complex structures, he had to ensure that they would not collapse. Therefore, studies about fracture mechanics have been made since a long time ago: Leonardo da Vinci performed strength tests on iron wires in 15th century, and Galileo Galilei was the first to give the correct scaling laws for bars under tension and bending in 1638.

Since fracture mechanics has a great economic importance, many studies were carried out in order to work out a theory that could explain the cracking behavior. The English aeronautical engineer A. A. Griffith showed the first quantitative results in his study entitled 'The phenomena of rupture and flow in solids' [25]: he investigated the energy balance in a material during the crack propagation. Subsequently, during World War II the scientist George Irwin added a significant contribute to the theory, recognizing the importance of the plastic zone during the crack propagation.

2.3. Modes of fracture

In fracture mechanics, three main modes of fracture are defined, as shown in figure 3:

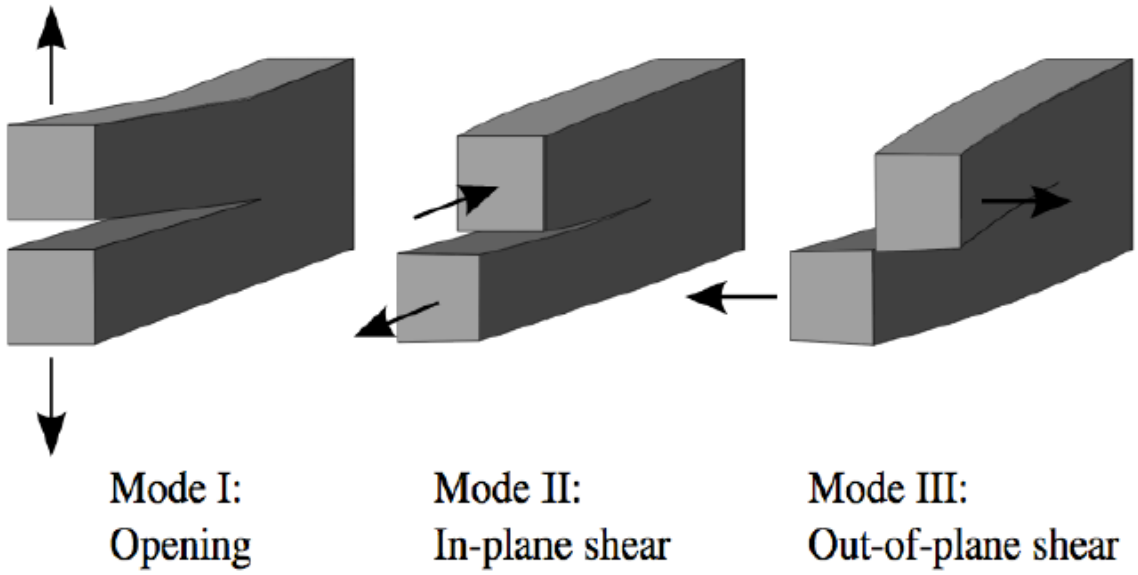

Figure 3. Modes of fracture

In this study, only mode I will be investigated. Mode I interlaminar delamination resistance is relevant since delamination is deemed an important failure mode.
Most load cases in structural applications of polymer-matrix composites involve mixed mode conditions; mode I is the worst-case scenario since it generally yields the lowest fracture toughness among other modes [26].

2.4. Failure analysis

The crack can propagate in three different ways in a composite material, as shown in figure 4 [27]:

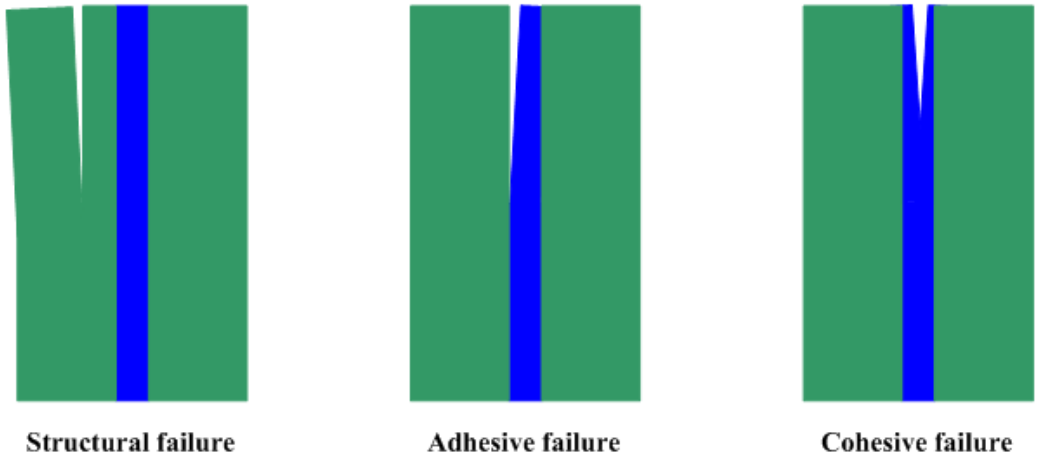

Figure 4. Types of fracture in adhesive-bonded composites [27]

- Structural failure: also known as delamination, the crack propagates between two layers of fibers.
- Adhesive failure: the crack grows at the interface between the bulk material and the interlayer.
- Cohesive failure: the crack remains inside the interlayer.

In addition to the failure loci, the mode of crack propagation is important and it may vary between different materials, different loads or different test velocity. The three main behaviors are shown in figure 5:

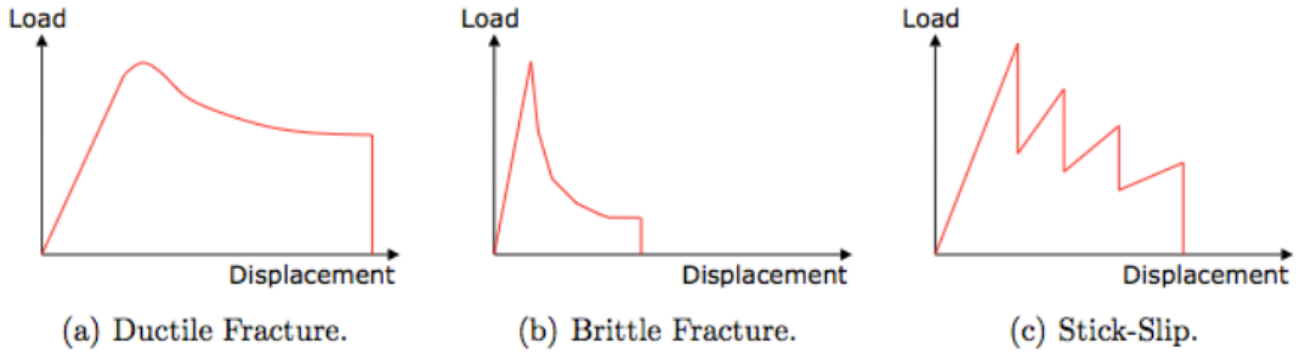

Figure 5. Load-displacement curves of different types of fracture

a) Ductile fracture is typical of metals, in which a significant plastic deformation is prior to failure;
b) Brittle fracture is typical of ceramics, where the absence of dislocations causes the failure without any plastic deformations.
c) Stick-slip behavior represents an unsteady propagation of the crack; in this mode of fracture, the crack grows in an intermittent way, making the crack length tricky to measure. In this case, the only possibility is to indicate the loads and displacements at the peak and at the arrest spot in order to evaluate the fracture toughness [28] [29].

2.5. Beam theory method of analysis

Griffith started from the assumption that the crack will grow only if the total energy of the system decreases. In order for the crack to propagate, the surface energy requirement for the new crack faces must be overcome by sufficient potential energy available on the plate. At the equilibrium, the change in energy for an incremental increase in the crack area A is equal to 0:

$$\frac{dE_t}{dA} = \frac{d\Pi}{dA} + \frac{dW}{dA} = 0 \quad (1)$$

Where E_t is the total energy, W is the work required for the creation of new surfaces; Π is the potential energy given by internal strain energy and external forces, which is calculated as follows:

$$\Pi = \Pi_0 - \frac{\pi\sigma^2 a^2 B}{E} \quad (2)$$

Where Π_0 is the potential energy of the plate without the crack, σ the applied stress, *a* is half the length of the crack, B is the thickness of the plate and E the Young's modulus.

The potential energy of an elastic body is also defined as

$$\Pi = U - F \quad (3)$$

Where U is the stored strain energy and F is the work done by the external forces.

Starting from the energy balance, Griffith considered a through-thickness crack in an infinitely wide plate subjected to a tensile stress:

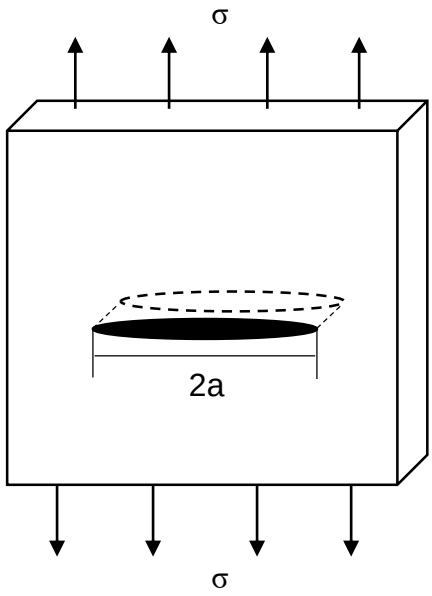

Figure 6. Stress applied in an infinitely wide plate

The calculations leaded to the Griffith equation which predicts the fracture strength σ_f:

$$\sigma_f = \left(\frac{2E_t\gamma_s}{\pi a}\right)^{\frac{1}{2}} \quad (4)$$

Where γ_s is the surface energy per unit area.

The application of this equation resulted in a good approximation of the behavior of brittle materials (glass) but also in a severe underestimation of the fracture strength of metals. For this reason, Irwin modified the Griffith's equation taking into account the plastic behavior of metals [30].

Irwin defined the Energy Release Rate G (also known as 'Crack Driving Force') as follows:

$$G = -\frac{d\Pi}{dA} \quad (5)$$

It is also defined the Fracture Resistance of a real material as:

$$R = 2W_f \quad (6)$$

where W_f is the work of fracture. Irwin's criterion states that the crack will grow if

$$G \geq R$$

G is calculated from the loading conditions, the elastic properties of the material (Young's modulus) and the specimen geometry; R is a material property that can be derived from fracture tests.

Therefore the crack will start to grow when G reaches a critical value G_c, where G_c = R.

Combining equations (2) and (5), and knowing that $dA = 2B\,da$

$$G = -\frac{d\Pi}{dA} = -\frac{1}{2B}\frac{d\Pi}{da} = \frac{\sigma^2 \pi a}{E} \quad (7)$$

The crack propagation will occur when

$$G = G_c$$

$$=> \frac{\sigma^2 \pi a}{E} = G_c \quad (8)$$

$$=> a_c = \frac{EG_c}{\sigma^2 \pi} \quad (9)$$

With equation (9) it is possible to evaluate the critical defect length that will cause fracture under a certain applied stress; nevertheless, it is necessary to determine the value of G. The calculation of G will be investigated under displacement control: in this case, the bottom face of a cracked plane is fixed and its top face is subjected to a fixed displacement (Δ) as shown in figure 7.

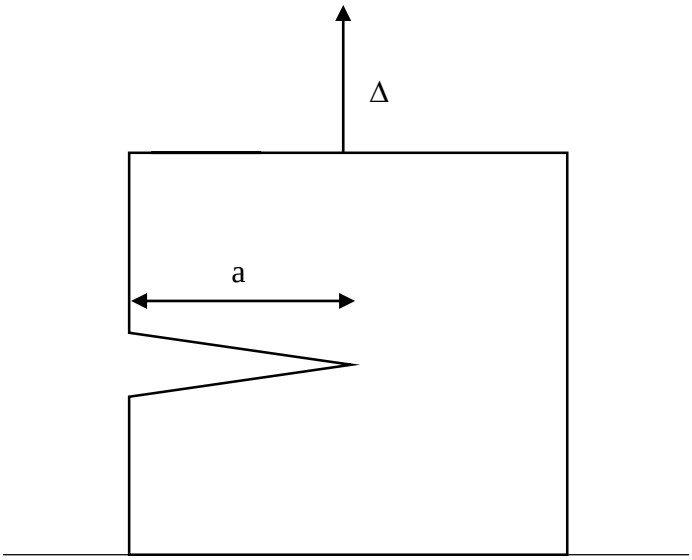

Figure 7. Schematic of mode I test

Since the displacement is constant, the work done by the external forces F is equal to 0. The equation (3) becomes

$$\Pi = U - F = U \quad (10)$$

The strain energy U is the area under the load (P) – displacement (Δ) curve:

$$U = \int_0^{\Delta} P d\Delta = \frac{P\Delta}{2} \quad (11)$$

With further calculations

$$G = -\frac{\mathrm{d}\Pi}{dA} = -\frac{1}{B}\frac{dU}{da} = -\frac{\Delta}{2B}\left(\frac{dP}{da}\right)_{\Delta} \quad (12)$$

It is convenient to introduce the compliance C, defined as

$$C = \frac{\Delta}{P} \quad (13)$$

Equation (12) becomes

$$G = -\frac{\Delta}{2B}\left(\frac{dP}{da}\right)_{\Delta} = -\frac{\Delta}{2B}\left(\frac{d}{da}\left(\frac{\Delta}{C}\right)\right)_{\Delta} = -\frac{\Delta^2}{2B}\left(\frac{d}{da}\left(\frac{1}{C}\right)\right)_{\Delta} = \frac{1}{2B}\frac{\Delta^2}{C^2}\left(\frac{dC}{da}\right)_{\Delta}$$

$$=> G = \frac{P^2}{2B}\frac{dC}{da} \quad (14)$$

Since this work is concerned with DCB tests, it is worth determining the value of G in case of DCB specimen, which can be assumed as a simple beam.
In DCB specimen, the displacement can be expressed as

$$\Delta = \frac{2}{3}\frac{Pa^3}{EI} \quad (15)$$

Where I is the moment of inertia, that for a rectangular section is

$$I = \frac{Bh^3}{12} \quad (16)$$

Using the definition of compliance

$$C = \frac{\Delta}{P} = \frac{2}{3}\frac{a^3}{EI} \quad (17)$$

$$=> \frac{dC}{da} = \frac{2a^2}{EI} \quad (18)$$

Combining equations (14) and (18) we obtain

$$G = \frac{P^2}{2B}\frac{dC}{da} = \frac{P^2a^2}{BEI} = \frac{12P^2a^2}{B^2Eh^3} \quad (19)$$

2.5.1. Corrected Beam Theory

SBT is related to built-in specimen, but it will underestimate the compliance in case the DBC specimen is not perfectly built in. For this reason a slightly longer crack length a + $|\Delta|$, where $|\Delta|$ is experimentally determined by plotting the cube root of normalized compliance $(C/N)^3$. N is defined as load-block correction and calculated as described below. In SBT, the hypothesis of small displacements is considered valid: in CBT, the displacement correction F is used and it contributes significantly if δ/a becomes larger than 0,4. N and F were investigated by Williams [31], and they are calculated as follows:

$$N = 1 - \left(\frac{l_2}{a}\right)^3 - \frac{9}{8}\left[1 - \left(\frac{l_2}{a}\right)^2\right]\frac{\delta l_1}{a^2} - \frac{9}{35}\left(\frac{\delta}{a}\right)^2 \quad (20)$$

$$F = 1 - \frac{3}{10}\left(\frac{\delta}{a}\right)^2 - \frac{3}{2}\left(\frac{\delta l_1}{a^2}\right) \quad (21)$$

where l_1 is the distance from the center of the loading pin to the midplane of the specimen beam and l_2 the distance from the center of the loading pin to its edge, as shown in figure 8.

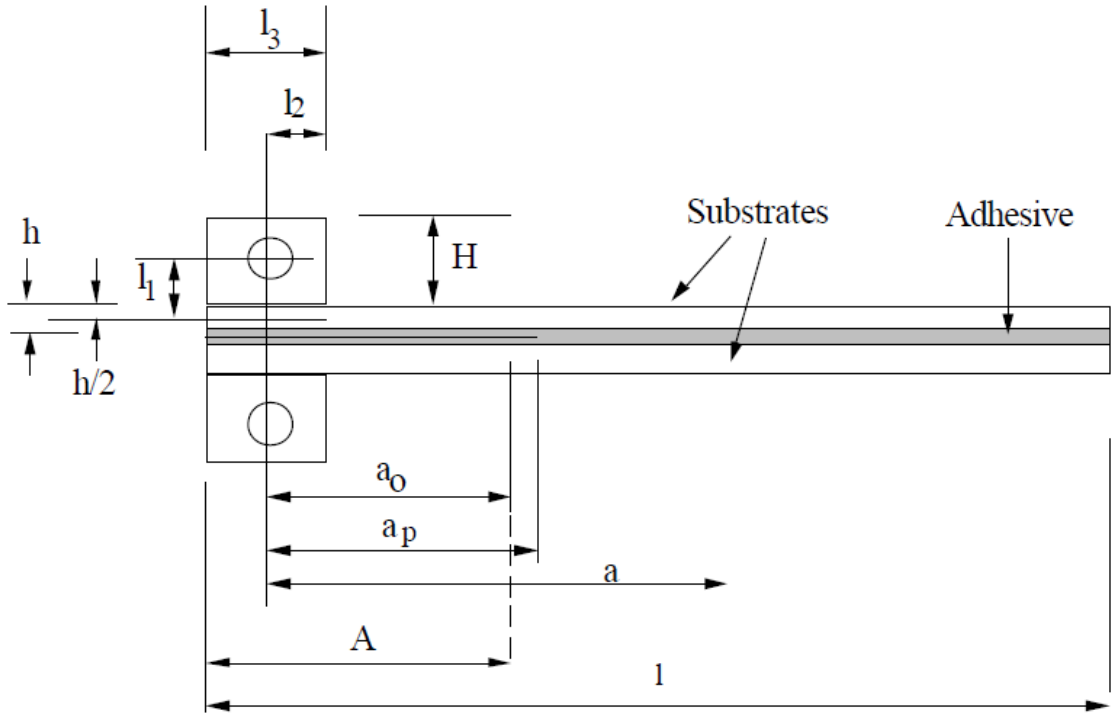

Figure 8. Dimensions in DCB test

The CBT approach allows to calculate the flexural modulus E_f:

$$E_f = \frac{8(a+|\Delta|)^3}{\left(\frac{C}{N}\right) Bh^3} \quad (22)$$

were Δ is the correction factor for the crack length, C the compliance, N the load blocks correction factor, B the width of the specimen and h half the thickness of the specimen. The flexural modulus obtained from this equation is used as a check on the procedure since it is independent of crack length. Normally the calculated value of E_f is larger than the modulus obtained from a flexural test.

2.5.2. *Stability of the crack propagation under fixed grip condition*

Crack growth will occur when $G = R$. The propagation will be either stable or unstable, depending on the variation of G and R during the phenomenon. Under fixed displacement, $\left(\frac{dG}{da}\right)_{\Delta}$ and $\left(\frac{dR}{da}\right)_{\Delta}$ are the subject of the investigation.

The fracture resistance R can be plotted against the crack length: the resulting graph is known as 'R-curve':

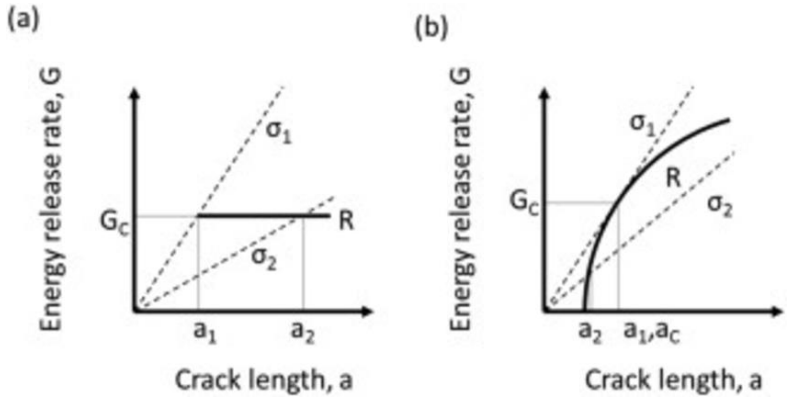

Figure 9. Flat and increasing R-curves [32]

The R curve shown in figure 6a is flat, and the value of G_c is constant regardless the length of the crack. This R-curve is typical of brittle materials, in which the surface energy is an invariant property of the material. Fig 9a shows that the lower the applied stress, the longer the crack length that will cause failure [32].

Figure 9b shows an increasing R-curve, which means that the value of R and consequently the value of G_c increase with the crack length. This R-curve is usually the result of ductile fracture: since the plastic deformation absorbs energy, the crack requires a higher driving force to grow. As shown in figure 6b, when the stress is equal to σ_2 the crack will grow a small amount, but then the value of R increases; for this

reason, it is necessary a higher stress in order to maintain the crack propagation, which remains stable.

When the stress reaches σ_1, the crack propagation becomes unstable since the slope of the energy release rate curve exceeds the rate of change of the R-curve. For this reason, it can be stated that the conditions for a stable crack growth are

$$G = R \quad \text{and} \quad \left(\frac{dG}{da}\right) \leq \left(\frac{dR}{da}\right)$$

The propagation becomes unstable when

$$G = R \quad \text{and} \quad \left(\frac{dG}{da}\right) > \left(\frac{dR}{da}\right).$$

2.5.3. *Stability of the DCB test*

From equation (15),

$$P = \frac{3}{2}\frac{EI\Delta}{a^3} \quad (23)$$

$$=> \left(\frac{dG}{da}\right)_\Delta = \frac{d}{da}\left(\frac{9E^2I^2\Delta^2}{4a^6} \cdot \frac{a^2}{BEI}\right) = \frac{d}{da}\left(\frac{9EI\Delta^2}{4Ba^4}\right) \quad (24)$$

$$=> \left(\frac{dG}{da}\right)_\Delta = -\frac{9EI\Delta^2}{Ba^5} = -\frac{4G}{a} < 0 \quad (25)$$

Since the derivative is negative, G will decrease with the crack propagation. For this reason, the test will remain stable and it will be possible to measure the crack length in order to determine the energy release rate.

2.6. Three-Point Bending test method

The three-point bending test consists of the application of an external load perpendicularly to the longitudinal axis of the specimen. This test is used to determine the flexural modulus of the substrate E: this value is necessary for the determination of the fracture toughness in the SBT theory: reminding equation (19),

$$G = \frac{12P^2a^2}{B^2Eh^3}$$

The standard that outlines the test method is ISO 14125:1998 [33]. In the standard, three-point bending test is referred as 'Method A' and it is suitable for fiber-reinforced thermoplastics.

The test configuration is shown in figure 10:

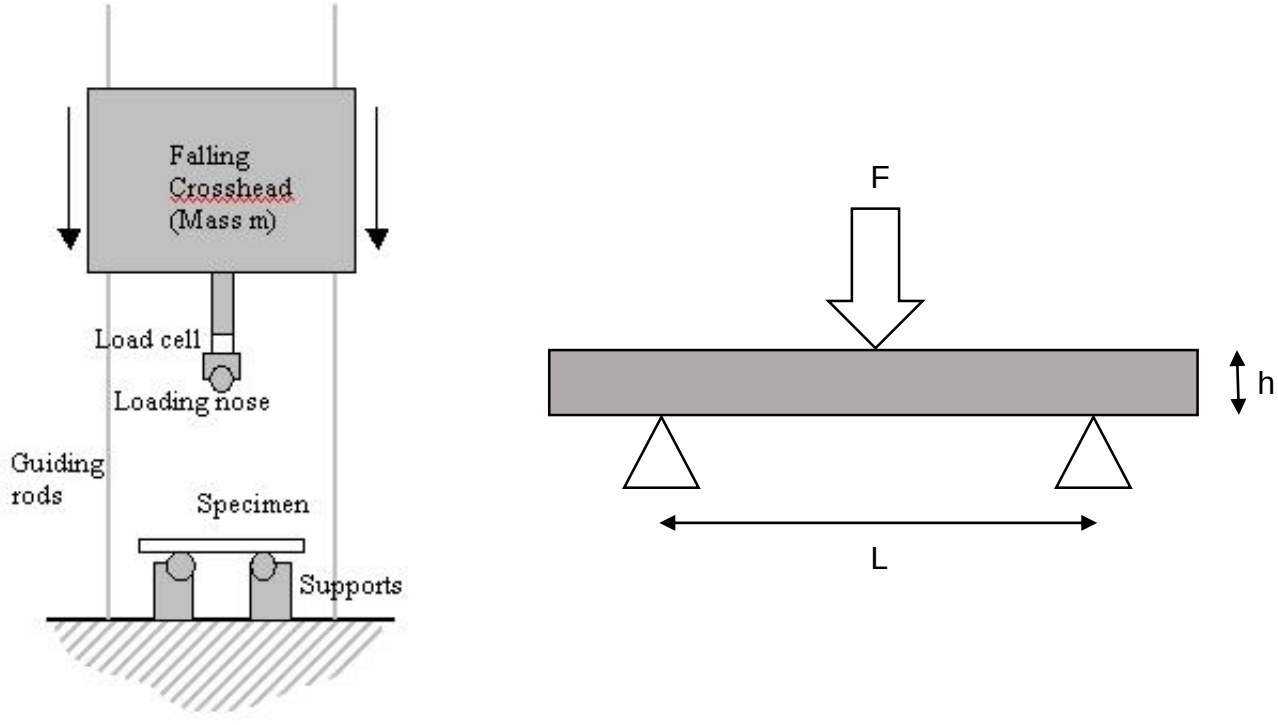

Figure 10. Three-point bending test [34]

The typical curve for a three-point bending test is given in figure 11:

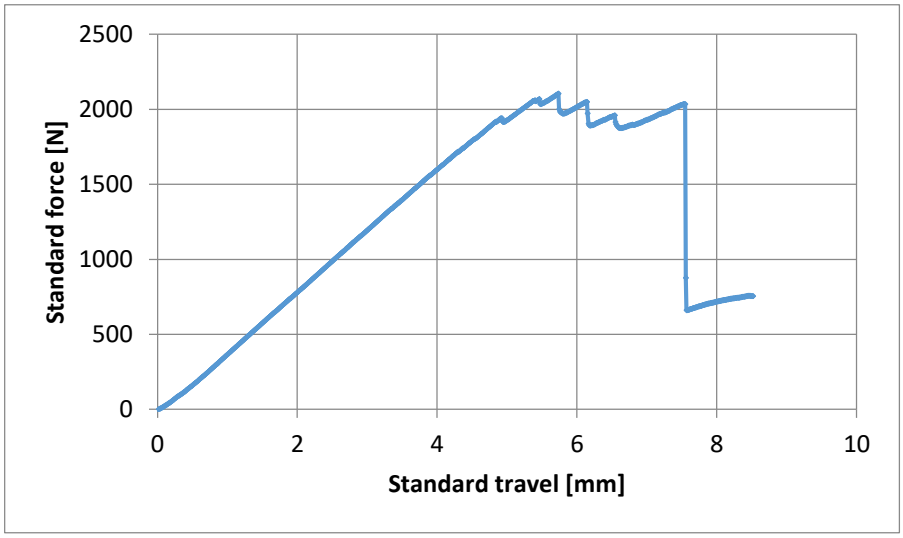

Figure 11. Typical load-displacement curve for three-point bending test

The slope of the initial linear part of the chart represents the flexural modulus of the specimen. The curve stops to be linear when rupture occurs: the force diminishes since the resistance of the sample is lower. When complete rupture occurs, the test is stopped and the data are analyzed.

From beam theory, the flexural stress σ_f is given by

$$\sigma_f = \frac{3FL}{2bh^2} \quad (26)$$

where

F is the load, in newton (N)

L is the span, in millimeters (mm)

b is the width of the specimen, in millimeters (mm)

h is the thickness of the specimen, in millimeters (mm).

For the determination of the flexural modulus, the two deflections s' and s" must be calculated: they correspond to the values of flexural strain ε'=0,0005 and ε"=0,0025 and the equation is

$$s' = \frac{\varepsilon' L^2}{6h} \quad (27)$$

and

$$s'' = \frac{\varepsilon'' L^2}{6h} \quad (28)$$

Once determined s' and s'', it is possible to calculate the flexural modulus E_f using the following equation:

$$E_f = \frac{L^3}{4bh^3}\frac{\Delta F}{\Delta s} \quad (29)$$

where

$\Delta F = F' - F''$, the loads respectively at s' and s''.

$\Delta s = s' - s''$.

The calculated value for E_f is then introduced in the equation for the determination of the fracture toughness using the simple beam theory; for the corrected beam theory, this value is not necessary since the flexural modulus is calculated from the load-displacement curve during the DCB test.

3. Materials

3.1. Chapter overview

This chapter describes the materials used in this project. The first part involves the description of the single materials used: fibers, resin and interlayers. The second part consists of the detailing of the manufacturing of the composites.

3.2. RTI overview

Resin Transfer Infusion method is a technique for the fabrication of composite materials developed and patented by Bombardier [35] in particular for the wings of Cseries and Learjet 85 airplanes [36].

RTI uses dry carbon fibers and resin that wets the fibers during the curing process. Differently from the Resin Transfer Infusion (RTM), RTI uses only one half of a mold to give the correct shape to the composite. The opposite outline is provided by a vacuum bagging material instead of injecting the resin inside the two halves of the tool (as in RTM). In this way, the surface quality of the final product is independent of the quality of the tool surface, which might be worn or damaged. The top lid is needed only to maintain the temperature inside the mold and to contain the air pressure.

In RTI process, two vacuum pumps and an autoclave are necessary to provide the curing atmosphere. In UCD lab, compressed air, the curing chamber and a heating system that is able to achieve 180 °C substitute the autoclave.

3.3. Composite

Reinforced composites are made up of a carbon fiber weave, which stiffens the polymer matrix.

Saertex, a company that supplies the dry fibers for the Bombardier Aerospace Aircraft Programme since 2011 [37], provides the fibers used in this project. Saertex fibers are non-crimped fabrics (NCFs), meaning that two different fiber orientation are stuck together but only stitching them instead of weaving them. The result is shown in figure 12:

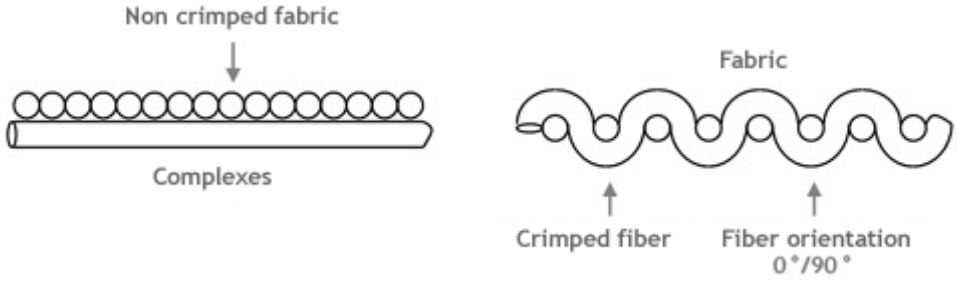

Figure 12. Non-crimped and crimped fabrics

According to Selcom [38], the advantages of non-crimped fabrics derive from the fact that the fibers are straight in their entire length. NCFs are able to minimize the risk of delamination and to maximize the tensile strength; a higher fiber volume fraction can be obtained, leading to higher mechanical properties compared to conventional (woven) fabrics.

Two different fiber configurations were available for this project: 0°/90° and ±45°. Figure 13 shows the 0°/90° configuration.

Figure 13. Detail of a fiber ply

The polymer matrix consists of epoxy resin (thermoset). The purpose of the polymer matrix is to transfer the load between the fibers and to support them under compression; the matrix contributes to lower the costs and to reduce the density of the final material.

The polymer matrix used in this project is CYCOM® resin, supplied by Cytec Company. It is stored in a refrigerator at -18°C in order to prevent it from curing.

3.4. Interlayers

The interlayers used in this project are thermoplastic materials. Thermoplastics are normally not used in composites since they have a lower melting point than thermosets; however, they have a higher fracture toughness than resin, therefore their use is believed to increase the fracture toughness of the composite. Four different materials were used in this project, and they will be discussed separately in the next chapter. The thermoplastics were in the form of a 0.05mm thick sheet, and they were provided by *Goodfellow Cambridge Limited*.

3.4.1. PolyImide (PI)

Polyimide is made of imide monomers. Because of its great performances at high temperatures (it is infusible), it is classified as *pseudo-thermoplastic* polymer. Polyimide has a transparent amber color. It is normally used for capacitors, insulation, water purification, and engine applications in aerospace industry.

The heat deflection temperature of PI is 360°C under a load of 1.8 MPa; since the temperature in the press clave reaches 180 °C, the thermoplastic will not melt inside the composite. The cost of PI is higher than the cost of other polymers used in this project.

3.4.2. Polyethylene Terephthalate (PET)

PET belongs to the polyester family. It is a hard, stiff, strong and dimensionally stable material with good gas barrier properties and chemical resistance. PET is common for food and liquid containers as well as for clothing, in the form of fibers.

The melting point for PET is 250°C [39]; as for PI, PET will not melt during the curing process.

3.4.3. Polyetherimide (PEI)

PEI is an amorphous, transparent plastic with characteristics similar to *polyether ether ketone* (PEEK). PEI is cheaper, less temperature resistant and lower in impact strength than PEEK. Because of its high durability and good insulation properties, PEI is widely used for circuit-breaker households and semiconductor components.

The melting point for PEI is 220 °C. *Akkerman et al* [40] measured the fracture toughness of PEI under quasi-static test condition: the value found was 3900 J/m^2.

3.4.4. *Polymethyl methacrylate (PMMA)*

PMMA is widely known for its commercial name, Plexiglas®. It is used in sheet form as a lightweight alternative for glass because of its high transparence, good surface finish and stiffness. PMMA is brittle in comparison with other engineering thermoplastics; hence, it was considered less promising than other thermoplastics like PEI since the beginning.

Polymethyl-methacrylate has a melting temperature of 160 °C; therefore, the thermoplastic will melt inside the composite.

3.5. Interlayer orientations

Beside the different materials investigated in this project as interlayers, three different orientations were trialed for each thermoplastic in order to establish the one that gives the best results. A schematic of each interlayer orientation can be seen in figure 14. The pink represents the PTFE thin sheet used as crack starter; the yellow stripes represent the thermoplastic interlayer.

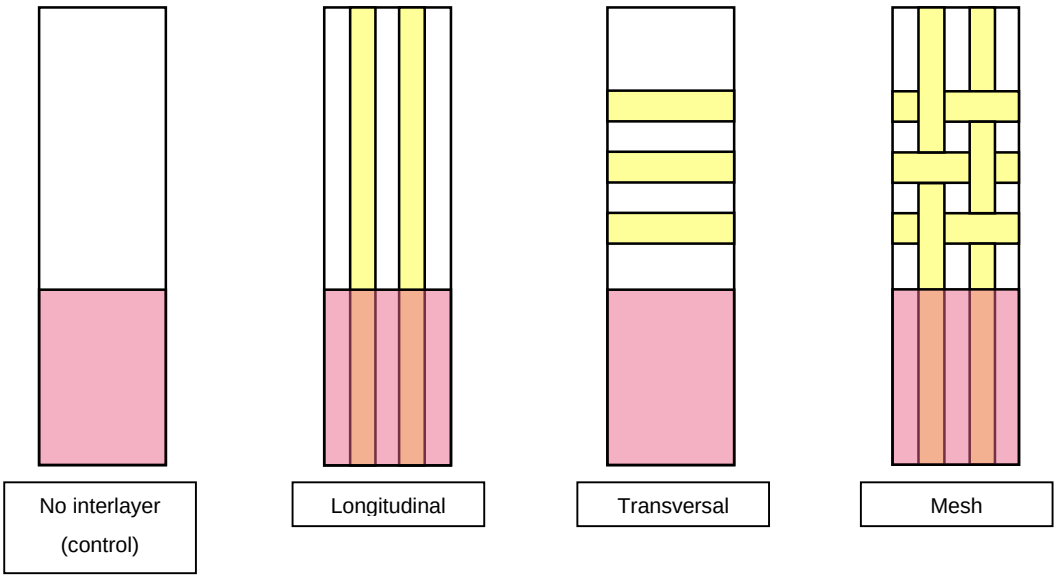

Figure 14. Interlayer orientations

3.6. Layup

The fiber rolls are cut in squares that measure 200x200 mm.

Before the layup, the interlayer is placed between two composite preforms, which consist of rolls with a 2-ply structure. As already mentioned, two different structure were available, the [0°/90°] and the [±45°]. In order to maximize the isotropic behavior of the laminate, four plies of fiber are used, each ply containing two layers of unidirectional fibers stitched together. The dry layup is constructed with the following configuration:

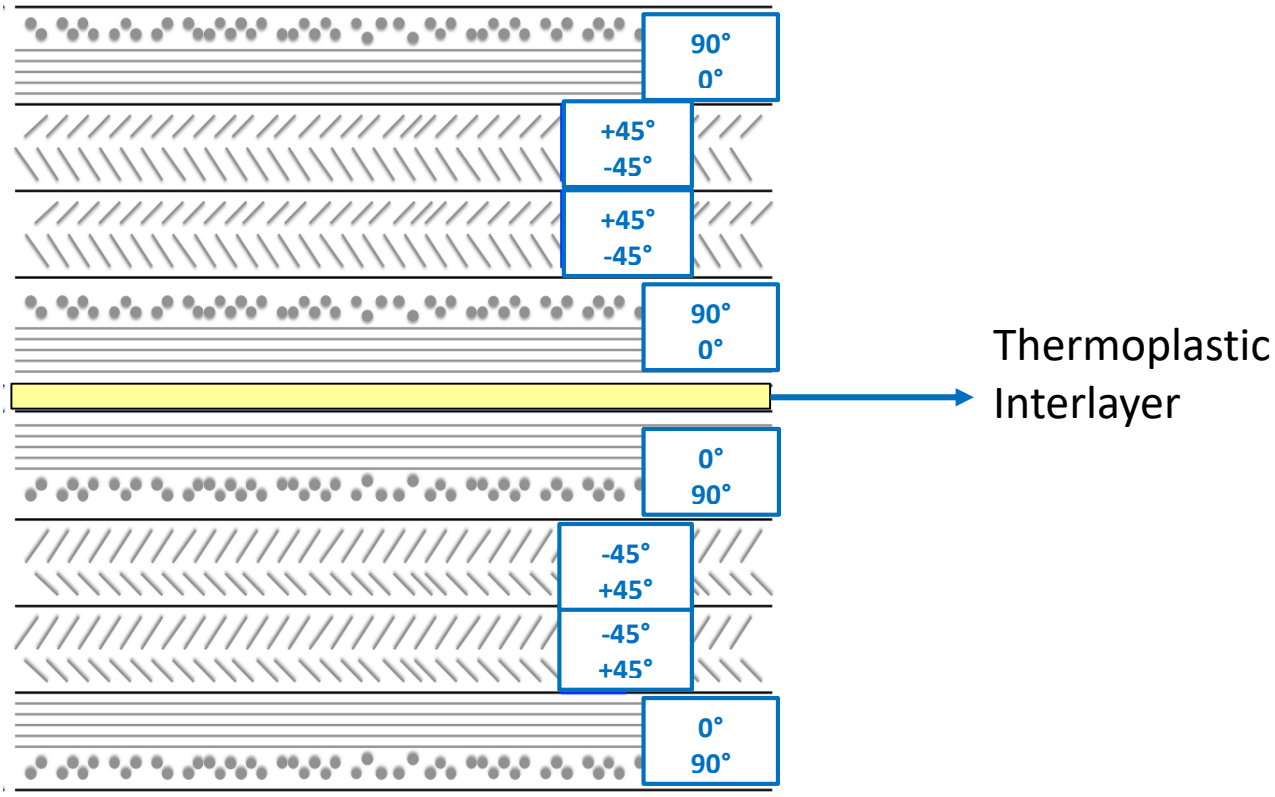

Figure 15. Fiber plies and interlayer configuration

Once the preform is ready, the layup can be made as desired. First, the mold is spread with Frekote 710 release agent in order to make easier the next operation of mold cleaning. Then a first sheet of PTFE is placed at the bottom, followed by a release ply.

These two sheets prevent the sticking of the composite on the mold and give a better surface finish.

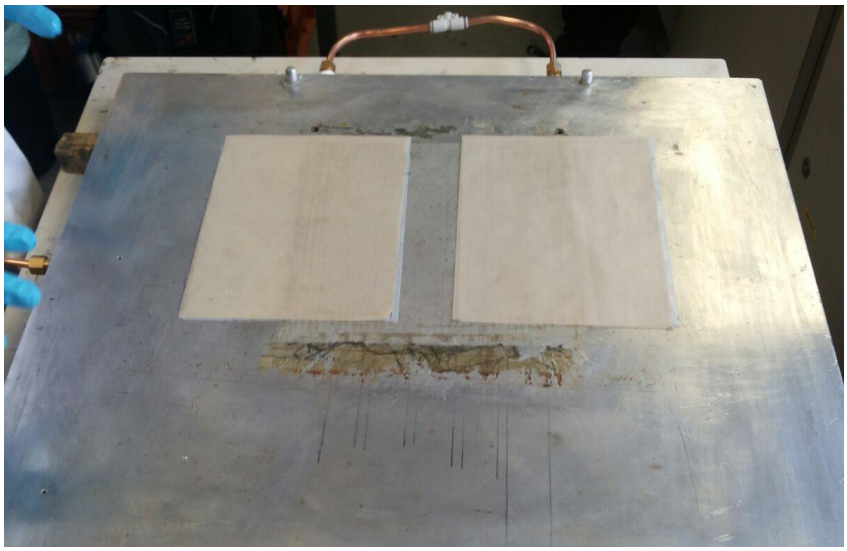

Figure 16. PTFE and release ply on the aluminium mold

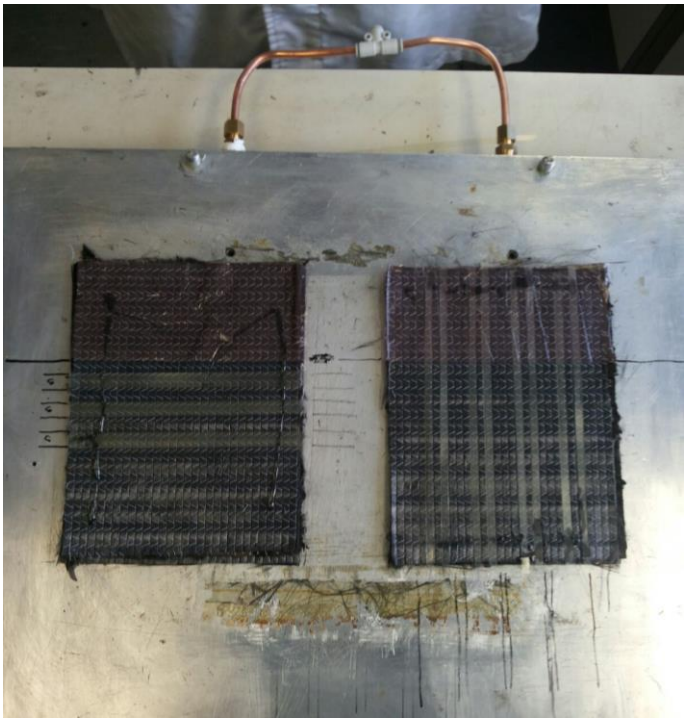

Figure 17. Fibers, PTFE crack starter (on top) and thermoplastic interlayer in form of transversal (left) and longitudinal (right) stripes.

After the release agent, the PTFE film and the release ply, the first preform consisting of four plies is positioned. Then, a 12 µm thick PTFE film is inserted as crack starter; after that, the interlayer is fixed on the top of the preform with the desired configuration (longitudinal, transversal or mesh). In order to maintain the interlayer in the correct position, it is stuck on the upper fiber ply using a drop of resin on each side of the strip. The second preform is placed over the interlayer. Afterwards, a release ply and a distribution mesh are positioned on top: the release ply helps the removal of the composite, whereas the distribution mesh (polyester) allows the resin to spread through the layup. The mesh has large gaps in between the strings: it is able to provide a path that is followed by the resin during the operation of cure.

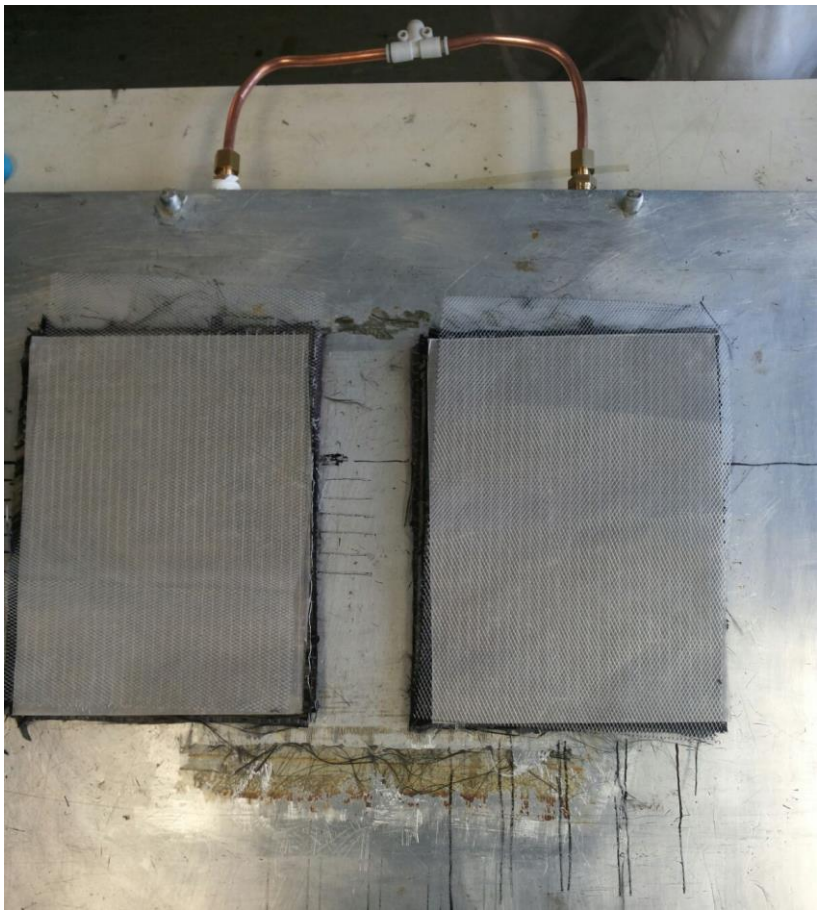

Figure 18. Release ply and distribution mesh over the fibers

The liquid resin is then displaced on the top of the distribution mesh. The correct quantity for this project is established to be 250g. Since the thermoset is very viscous and sticky, it is poured in a bowl covered with a PTFE sheet; the PTFE is then removed and turned upside down in order to place the resin in contact with the layup.

After these operations, the first vacuum bag can be sealed using a temperature resistant sealant tape: the bag covers the layup and two holes that are connected to the vacuum pump. The vacuum is activated and the bag is checked in order to avoid any possible leaks in the sealing system.

Figure 19. Inner bag with sealant tape (yellow). Breather visible on the right

Once the first vacuum bag is checked, a breather fabric is placed on its top; this layer helps the pressure to be uniformly distributed on the composite. A second vacuum bag is then positioned over the entire structure: this vacuum bag is meant to work for the entire curing period. After the removal of any leaks of the second bag, the top lid is placed and the mold inserted in the press clave.

The entire configuration of the system can be seen in figure 21:

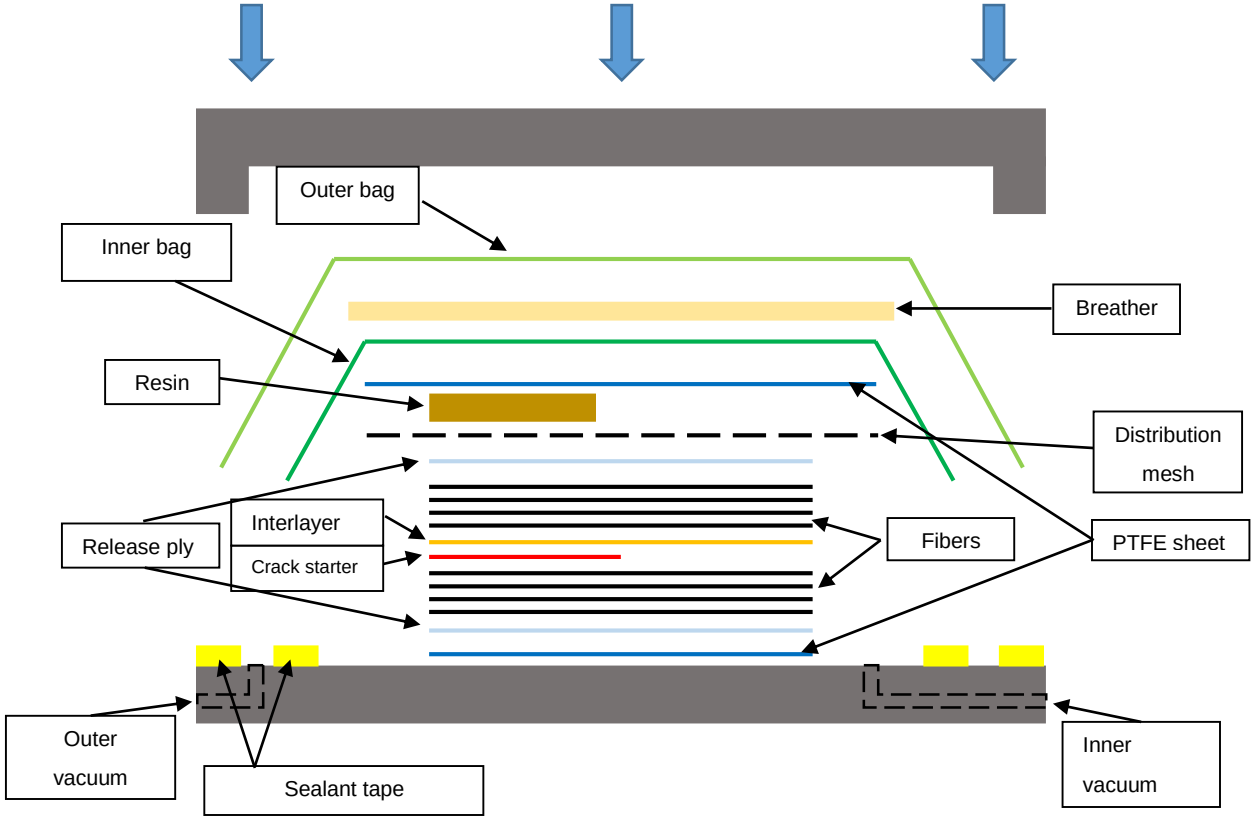

Figure 20. Complete configuration of the system

Activating the thermocouples, the process starts. It consists of a 2 hours ramp to reach 180 °C; then the temperature is held at 180 °C for 2 hours.

After about 1 hour from the beginning of the process, when it reaches a temperature of about 110 °C, the resin starts to flow out from the first vacuum bag. The excess resin can be seen in the transparent pipe that connects the clave and the vacuum pump: when the resin reaches 70 cm in the vacuum pipe, the pump is turned off and the process continues without the inner vacuum. In order to replace the vacuum and

to assure a homogenous pressure distribution, compressed air is applied at a pressure of 6 bar; in addition, the load of the press is increased to 550 kg.

After the heating cycle, the thermocouples are automatically switched off and the system cools down overnight without any process control.

The morning after, the mold is removed from the press-clave. After the removal of the top lid, the vacuum bags and the other outer layers are peeled away and the final composite plate is obtained.

4. TESTING METHODS

4.1. Chapter overview

In this chapter, the testing methods and equipment are described from the preparation of the sample to the typical results for the tests.

4.2. Sample preparation

The composite plate after the curing process measures 200x200 mm. After its removal from the clave, it is cut using a diamond coated grinding wheel from a tile cutter in the workshop. Since the edges of the composite plate are not straight due to the uneven flow of resin, a metal bracket is used to define a straight line. After the cutting of the edges, the specimens are cut taking into account that the width of the blade is 2.2 mm. The dimensions of the DCB specimens are 150mm in length and 25mm in width; the length of the crack starter is 57,5mm. From the 200x200 mm plate, four samples are obtained: this number of samples is sufficient to determine the fracture toughness avoiding any possible machine errors.

After the cutting process, the samples are cleaned from the dust. The specimens for the three-point bending test require no further preparation.

Since during the DCB test the crack length must be monitored, the DCB samples need to be marked in their length. First, two aluminium blocks are glued onto the specimens using a structural adhesive: the loading machine will apply the tensile load through the blocks. The blocks have a hole in their center, where the pin will be inserted in order to connect the loading machine and the sample.

Once the adhesive is cured, the specimens are marked in their length. First, one side of the samples is coated with white correction fluid ‘Tipp-Ex’: with a white background it is easier to visualize the crack.

After a few minutes the white fluid is dried and the side of the specimen is marked using a pen with a 0.1 mm nib diameter. The first black mark is placed at the edge of the crack starter, at 57,5 mm from the edge of the specimen. Then five red marks are drawn every 1 millimeter, followed by 10 black marks every 1 millimeter. After these, other black ticks are drawn every 5 mm for the next 50 mm; at the end, the last five mm are marked with a black mark every 1 mm. The final result is shown in figure 21:

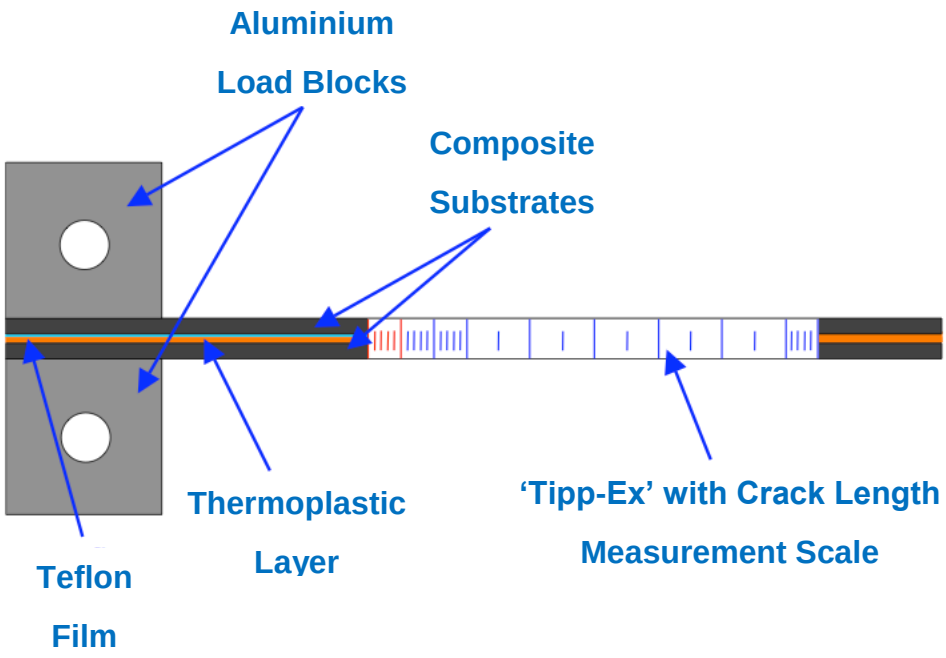

Figure 21. DCB specimen characteristics

For SBT and CBT theories, it is important to specify the measures of the specimen that are shown in figure 22:

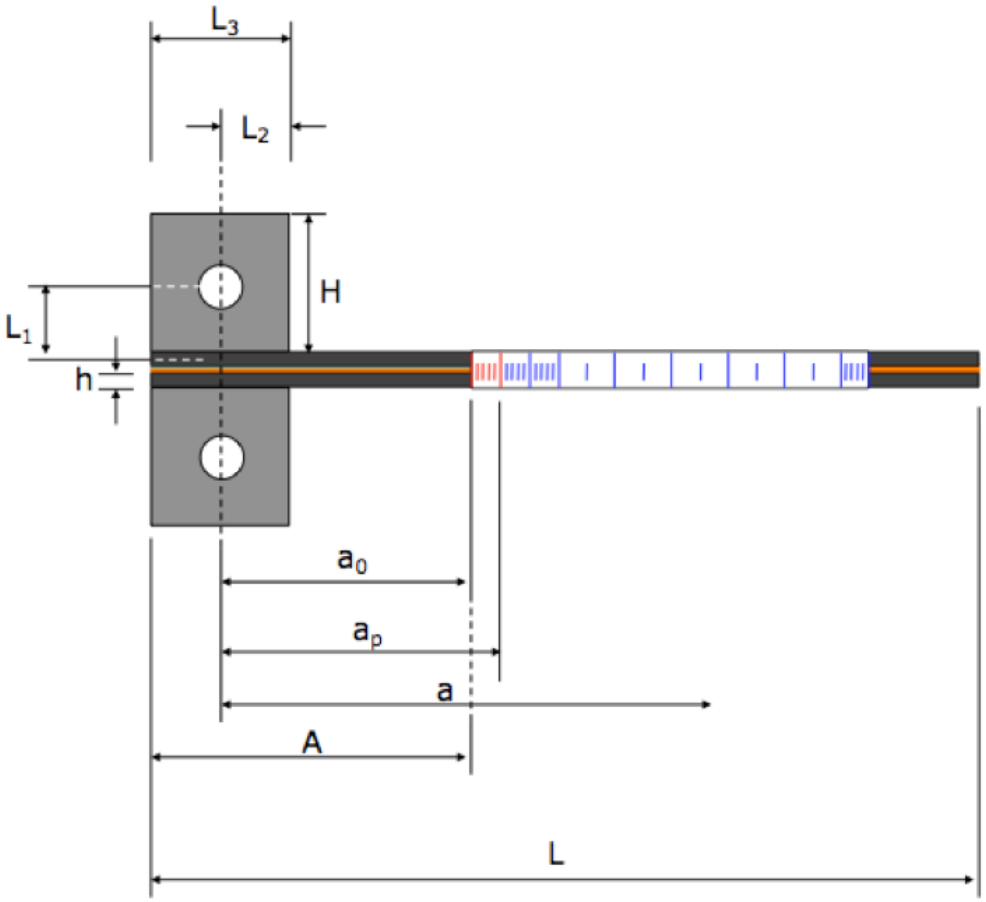

Figure 22. Dimensions in the DCB specimen

Table 1 shows the values of the lengths in figure 22:

L	L_1	L_2	L_3	A	a_0	H
150	13.9	12.5	25	57.5	45	25

Table 1. DCB dimensions

4.3. Three-Point Bending test

The DCB test method is standardized by British Standard Institution (BSI). The standard BS 7991:2001 outlines the procedure for the “Determination of the mode I adhesive fracture energy G_{IC} of structure adhesives using the double cantilever beam (DBC) and tapered double cantilever beam (TDCB) specimens” [41]. The method used in this project follows precisely the indications given in the standard.

The three-point bending test is carried out using an *Instron 8501* series. Since this test is necessary for the determination of the flexural modulus of the substrate, it is carried out using specimen with neither a thermoplastic interlayer nor the Teflon crack starter. Five specimens were used for the three-point bending test in this project.
Figure 23 shows the apparatus: the span is 96 mm and the dimensions of the specimens are the same as the DCB specimens, 150x25 mm.

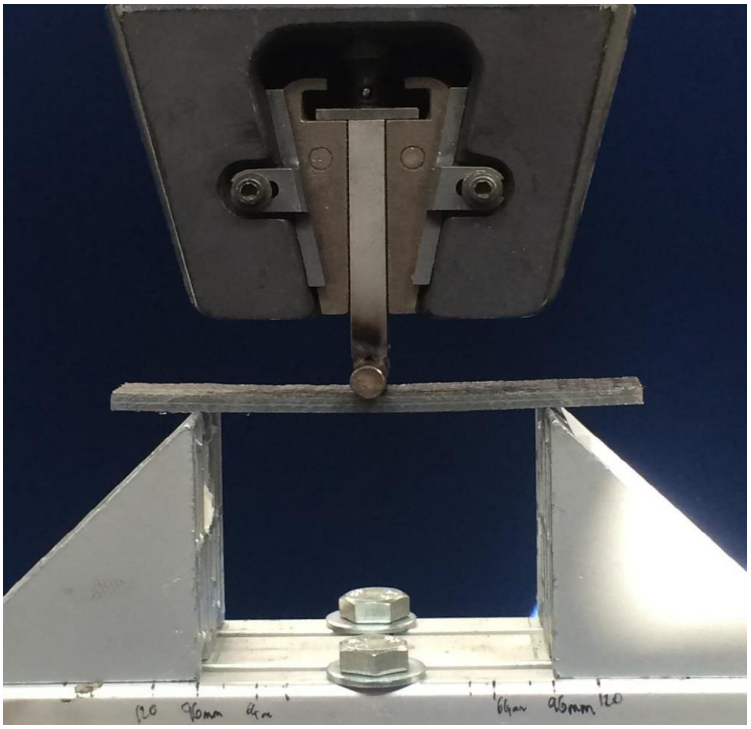

Figure 23. Three-point bending test apparatus

While the load is being applied, the software records the results of the test in a load – deflection curve: the flexural modulus is the slope of this curve and it is calculated using equation (29).

4.4. Double Cantilever Beam test

The DCB test is carried out with a *Hounsfield* tensile tester and a *Qmat* software. First, the specimen is mounted into the tester grips through the aluminium blocks. A loading cell of 10 kN was employed, allowing the real time measure of the load. As already mentioned in chapter 2.5.3, for stability reasons the test is carried out at constant displacement: the chosen velocity for the DCB test was 2 mm/min.

Before the test, the width and the thickness of each specimen is measured at the two edges and at the center using a caliper with an accuracy of 0.01 mm. The mean value of those measures was used for the determination of the fracture toughness.

When the Hounsfield is started, an Excel macro is started at the same time. This macro was developed by the Imperial College London, and it allows the determination of the time at which the crack reaches the marks on the specimen.

When the tensile load is applied, the crack propagates through the preferential direction given by the crack starter, which means in the midplane of the composite; the crack length is monitored using a travelling optical microscope with a magnification of 10x.

The loading procedure and the testing apparatus is shown in figure 24.

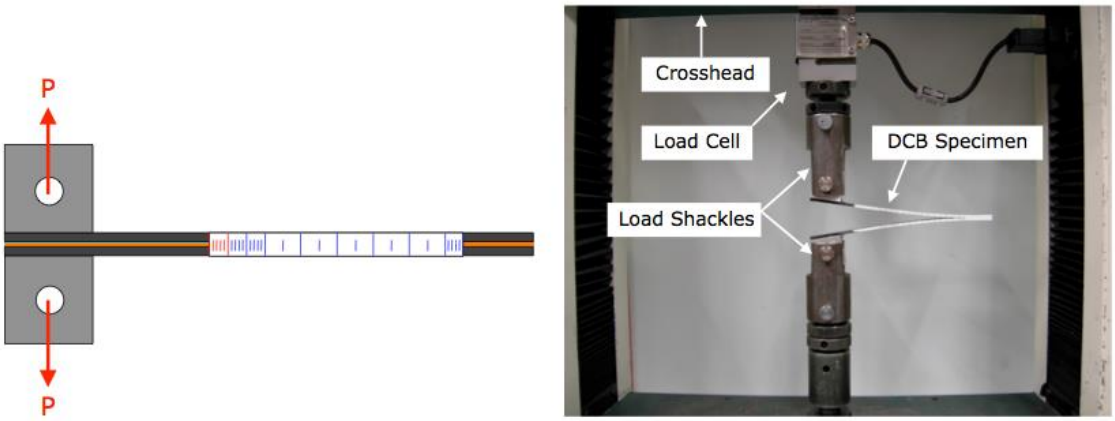

Figure 24. DCB test apparatus

The DCB test is divided into two parts, as specified by Blackman and Kinloch [28]. At first, the sample is loaded and the crack starts to propagate; when it reaches the last red mark (5 mm beyond the edge of the crack starter), the test is stopped and the sample is unloaded. This first phase is named ‘Insert’: it helps the crack to grow in the correct direction and assures a correct tip shape [28].

The second phase is known as ‘Precrack’. The sample is reloaded and the crack overcomes the length that it had reached in the insert; it propagates until rupture occurs. A sample undergoing the DCB test is shown below:

Figure 25. Specimen undergoing the DCB test

For both insert and precrack, when the crack reaches each tick the length is recorded in the Excel macro; the time is automatically recorded by the macro itself. At the end of the test, the loads are obtained from the Qmat software, which plots a load-displacement curve. The loads are then transferred in the macro that is able to plot a load-displacement curve that comprehends the crack lengths recorded during the test.

4.5. DCB test typical results

A typical result of the test is shown in figure 26:

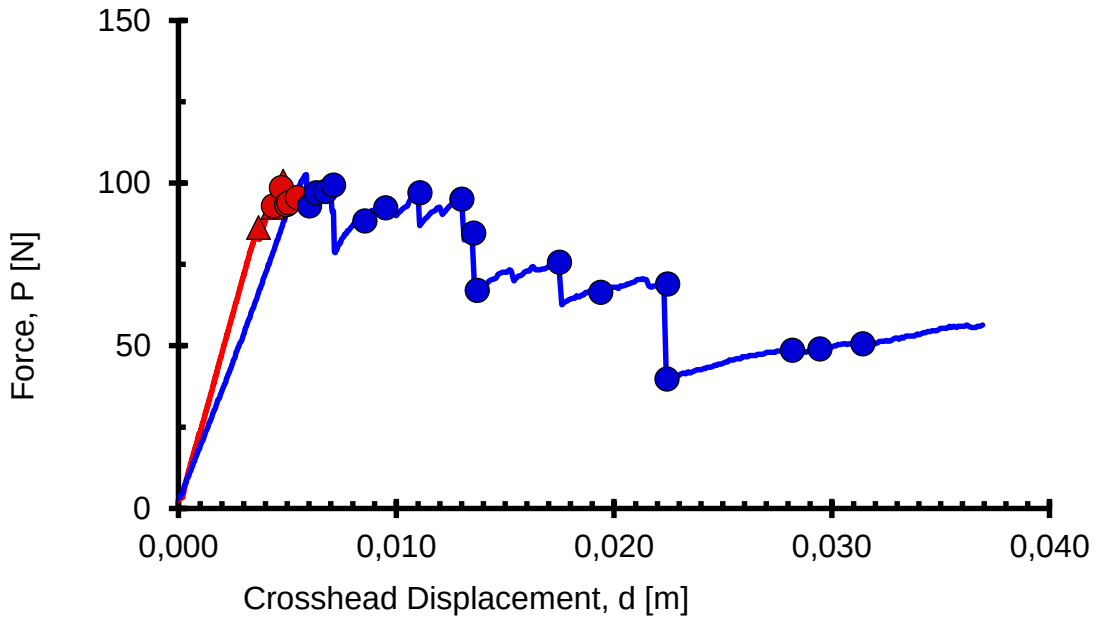

Figure 26. Typical load-displacement curve for DCB test

In this chart, the red line represents the insert and the blue line represents the precrack. The red and blue dots represent the propagation point that coincide with the marks on the side of the specimen.

Observations of stick-slip behavior were reported in many of the tested samples: for this reason, it was tricky to exactly determine the crack length at each point of the test.

Stick-slip is the result of the alternation between sticking and sliding of the two crack surfaces; in the case of crack ‘jumps’, the method that is normally used is to find the arrest and the initiation points on the force-displacement chart as shown in figure 27 [42]:

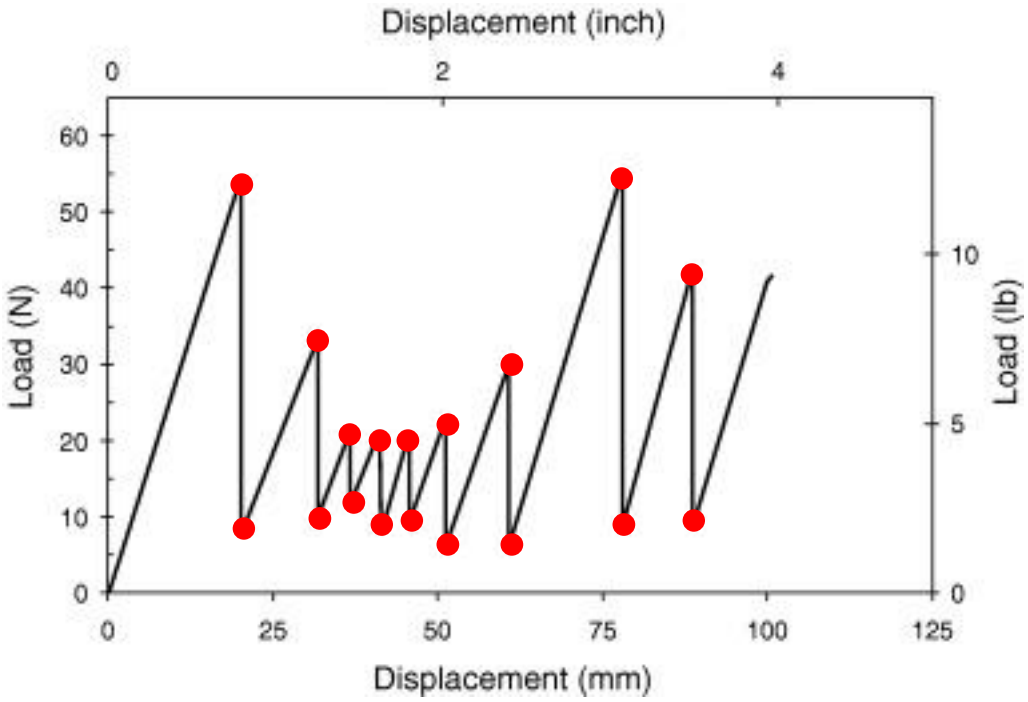

Figure 27. Typical load-displacement curve in a stick-slip behavior [42]

The instability of the load-displacement curve is the basis of the fluctuation of values in the fracture toughness-crack length curve. The red dots are usually determined at the end of the test since the correct evaluation of the crack length during the test is hard to carry out.

4.5.1. Initiation and propagation points

Initiation and propagation points are necessary for the calculation of the fracture toughness [41]. The following points are to be determined:

- NL: the point of deviation from linearity;
- VIS: the point at which the crack is observed to grow from the tip;
- $C_{0+5\%}$: the point at which the compliance has increased by 5%.
- MAX: the maximum point between the $C_{0+5\%}$ point and the maximum of the first linear region.
- PROP: the propagation points, as already mentioned, coincide with the ticks placed on the side of the samples.

A schematic of the initiation and propagation points is shown in figure 28. In this case, the MAX and $C_{0+5\%}$ points coincide.

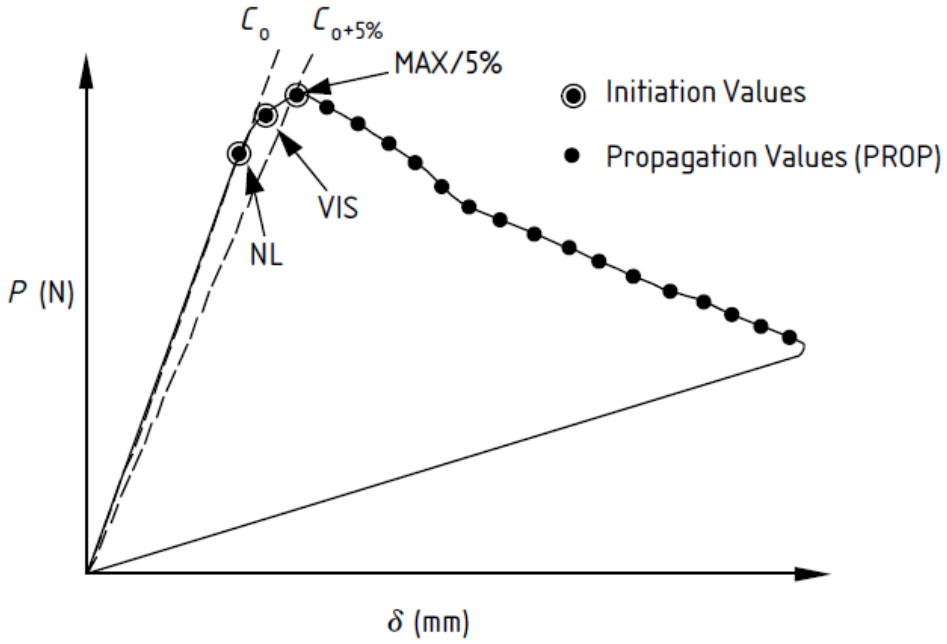

Figure 28. Initiation points in a load - displacement curve [41].

For each point, the load and the displacement are recorded and inserted in an Excel sheet developed by the *Imperial College London*. The calculation sheet, once provided all the initiation and propagation points, the thickness and the width of the specimen, the cross speed value and the slope of the linear region automatically calculates the fracture toughness G_{IC}.

4.5.2. R-curves

As already mentioned in chapter 2.5.2, composite materials normally show non-constant R-curves, meaning that the resistance to the crack propagation changes with the crack growth. For this reason, in this project it is interesting to show the fracture toughness in relation to the crack length: a typical result is shown below:

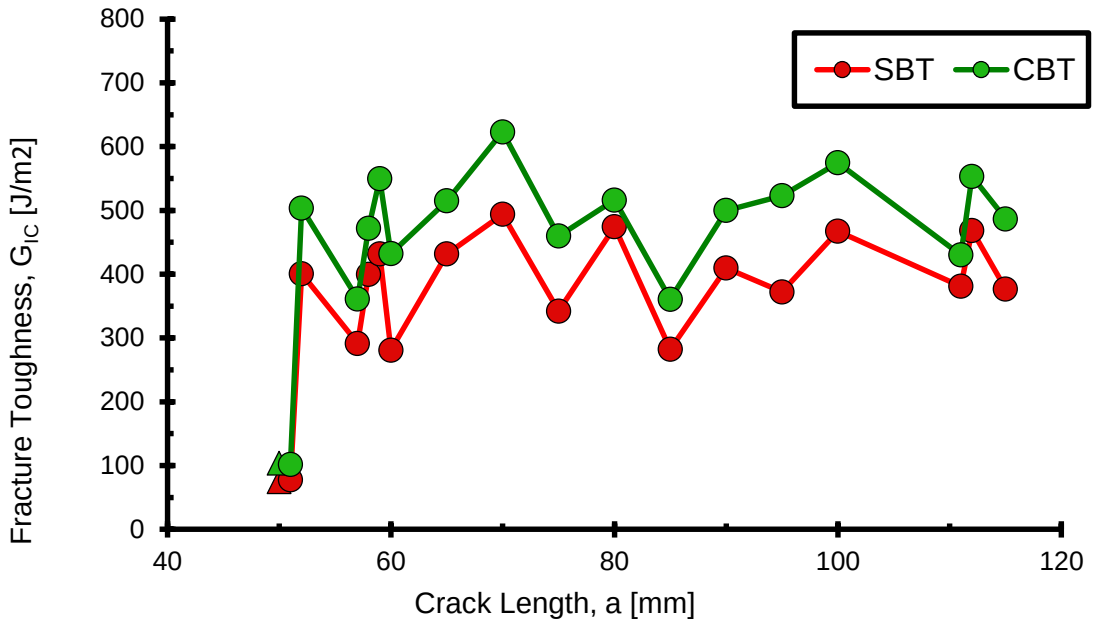

Figure 29. R-curves for CFRP

It is evident how the toughness changes during the propagation of the crack: when the variation of the values of G_{IC} is high, it makes no sense to calculate its mean value since this value would not be representative of the overall behavior of the composite. For this reason, scientists normally show the R-curve instead of the value of the fracture toughness [43].

5. Results

5.1. Chapter overview

Chapter 5 comprehends the results obtained with the three-point bending test and the DCB tests. As regards the DCB results, they are divided by material, and a comparison is made between the different materials and the different configurations.

5.2. Three-point bending test

The value of the flexural modulus found with the three-point bending test was 32 GPa. This value is low compared to the result obtained by John Mohan using the UCD apparatus [24]. After the data analysis further tests were carried out manufacturing more samples, but the results obtained were consistent with the ones coming from the first plate.

Since this project was neither about the precise determination of the flexural modulus nor the increasing of the modulus itself, this test was considered valid and the value of 32 GPa was used in the SBT calculations. Since the modulus of the core material is the same for the specimens without interlayer and the ones with the thermoplastics, it is considered that this low flexural modulus does not affect the influence of the strips on the fracture toughness.

It is probable that the cause of this reduction is the non-uniform distribution of the resin throughout the entire plate.

5.3. DCB test

The results are worked out using both SBT and CBT. Since CBT takes into account the effect of the load blocks, the rotation of the beam during the test and the large displacement it is considered more accurate and therefore the results will be discussed in terms of CBT values.

5.3.1. No interlayer

The specimens without thermoplastic interlayer are used as reference in order to evaluate the effectiveness of the interlayer; four specimens without interlayer were tested. The load-displacement curve for the no-interlayer specimen 3 is shown in figure 30.

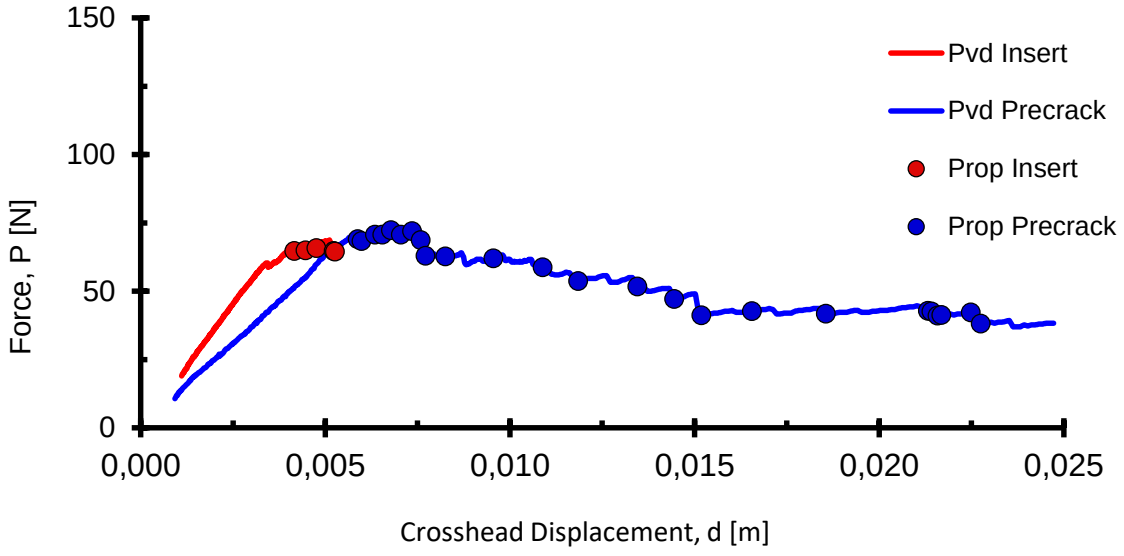

Figure 30: Load-displacement curve for no interlayer specimen 3

The stable propagation of the crack leads to nearly flat R-curves, shown in figure 31:

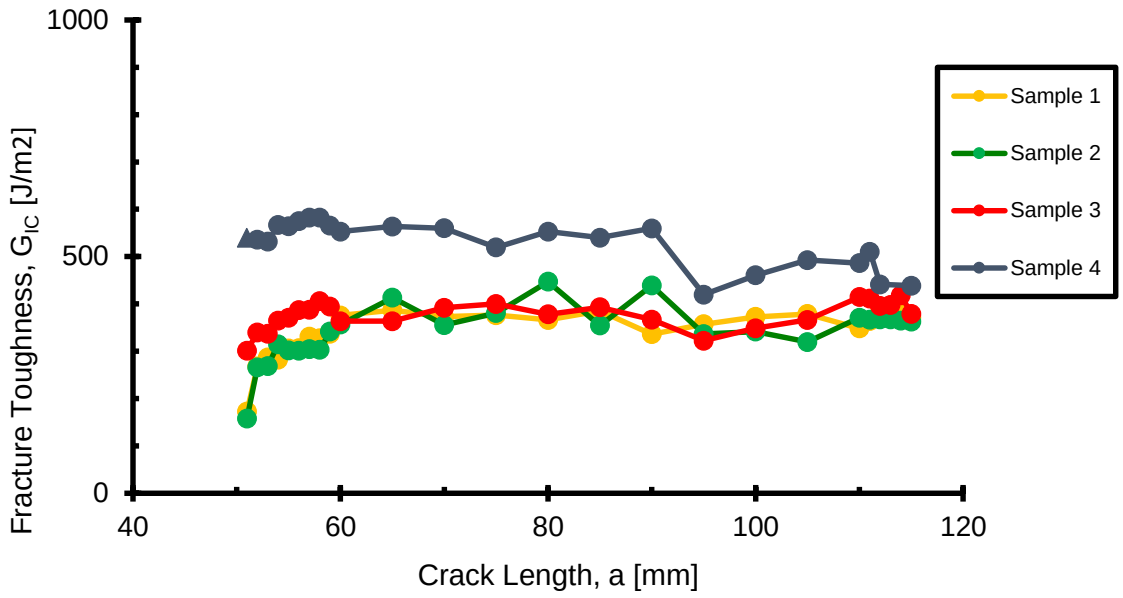

Figure 31: R-curves for specimens without interlayer

The R-curves show small fluctuations of values for each specimen.

Since the propagation of the crack occurs with regular behavior, and the R-curve has small fluctuations of values, the average value of G_{IC} is calculated and it is considered representative of the toughness of the specimens. The mean values for each specimen and the overall mean value for specimens without interlayer are shown in figure 32.

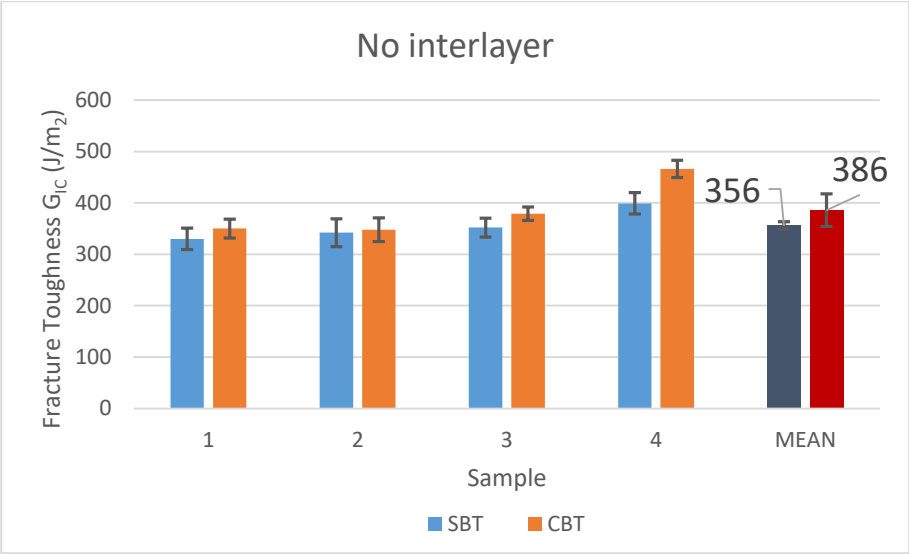

Figure 32: Fracture Toughness for specimens without interlayer

The value of 386 J/m^2 is used as reference.

Figure 33 shows that cohesive failure occurred in specimen without an interlayer present.

Figure 33: The interface at which failure occurred in a specimen with no interlayer.

The fracture occurs between the two layers of fibers separated by the crack starter: the crack is able to continue its path since there are no 'obstacles'.

5.4. Polyimide (PI)

5.4.1. PI longitudinal strips

The crack propagation was observed to be regular. There are only small 'jumps' of the crack, and the fluctuations of G_{IC} values are small; for this reason, the mean value of the fracture toughness is calculated and it is considered representative of the overall behavior of the composite. The stability of the crack propagation is visible in figure 34.

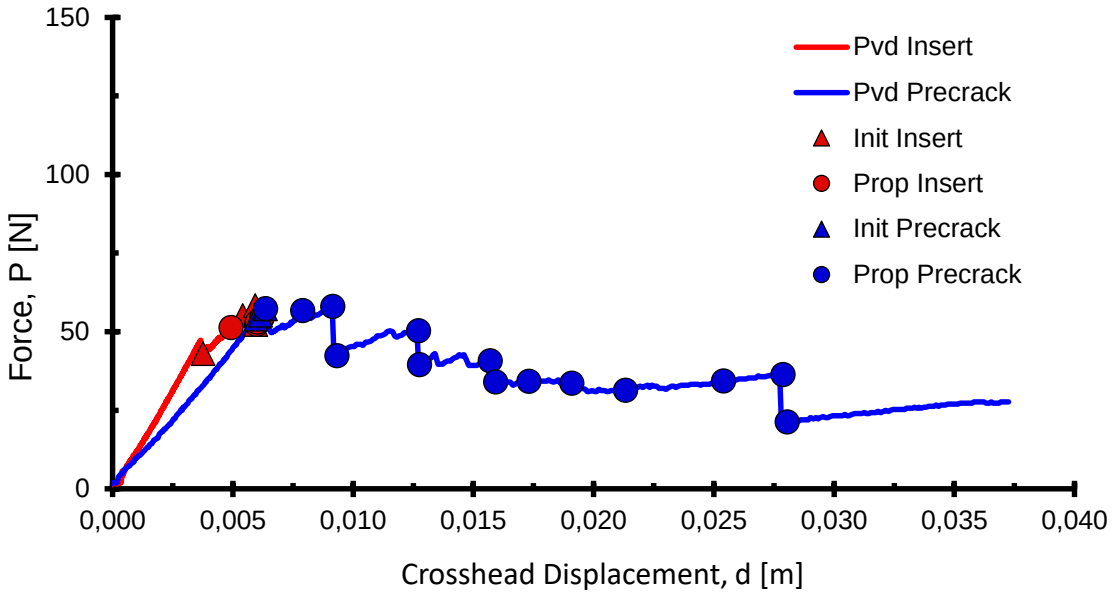

Figure 34. Load-displacement curve for PI longitudinal strips specimen 3

As already found with the specimens without an interlayer, the stable growth of the crack leads to stable R-curves, shown in figure 35.

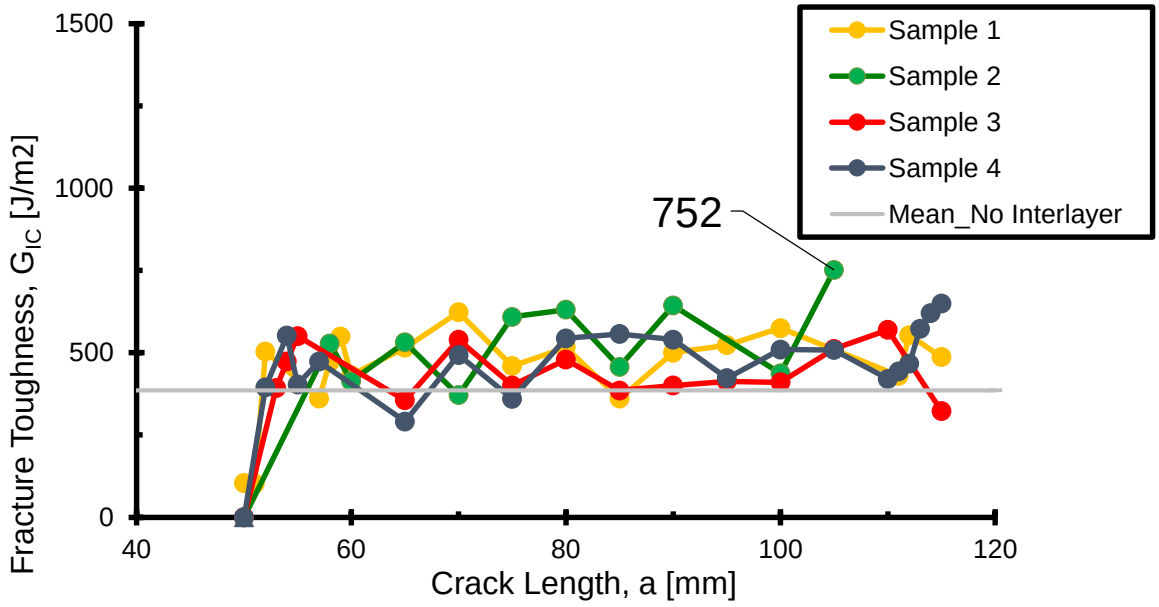

Figure 35. R-curves for PI longitudinal strips specimens

The increasing of fracture toughness provided by the addition of PI longitudinal strips is shown in figure 36.

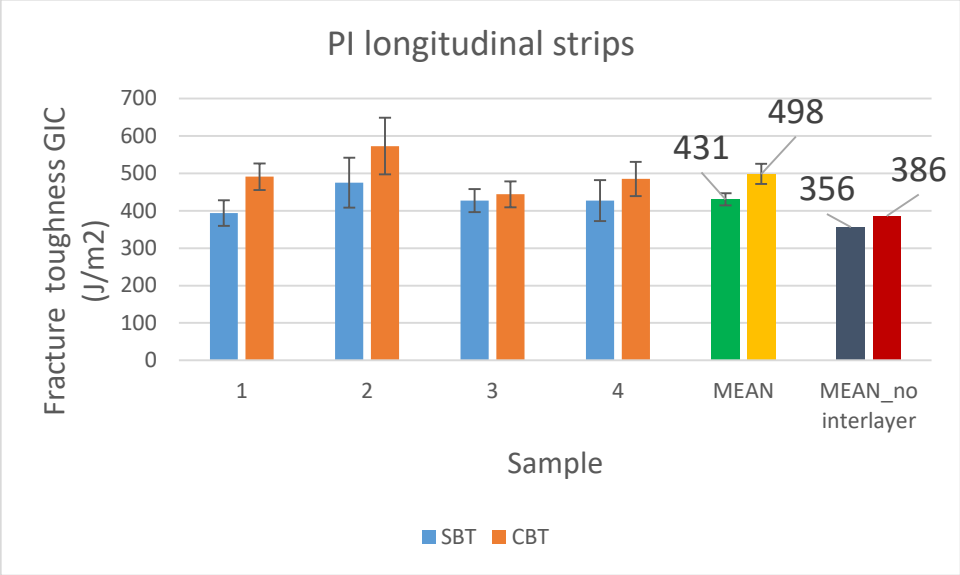

Figure 36. PI longitudinal strips results

Taking into account the CBT values, the fracture toughness is increased by around 100 J/m^2 using the PI longitudinal strips. Looking at the surface of failure, the fracture is observed to be cohesive:

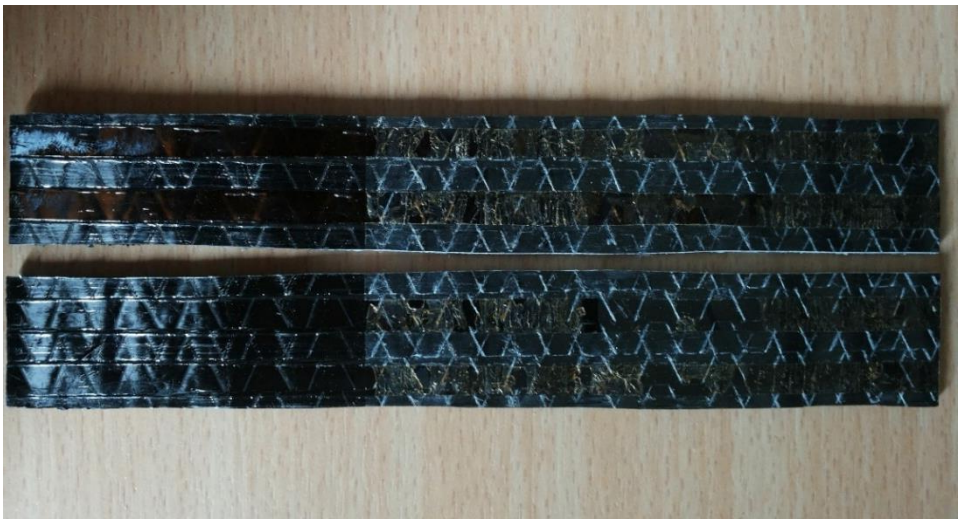

Figure 37. PI longitudinal strips specimen 3

The longitudinal thermoplastic strips are still clearly visible on both sides of the specimen: this means that the crack proceeded through the thermoplastic, confirming that the fracture was cohesive.

5.4.2. PI transversal strips

The crack propagation was observed to be irregular. This irregularity is due to the crack-stopping action of the thermoplastic strip, as already stated.

In figure 38, the load-displacement curve for specimen represents the instability of the crack growth:

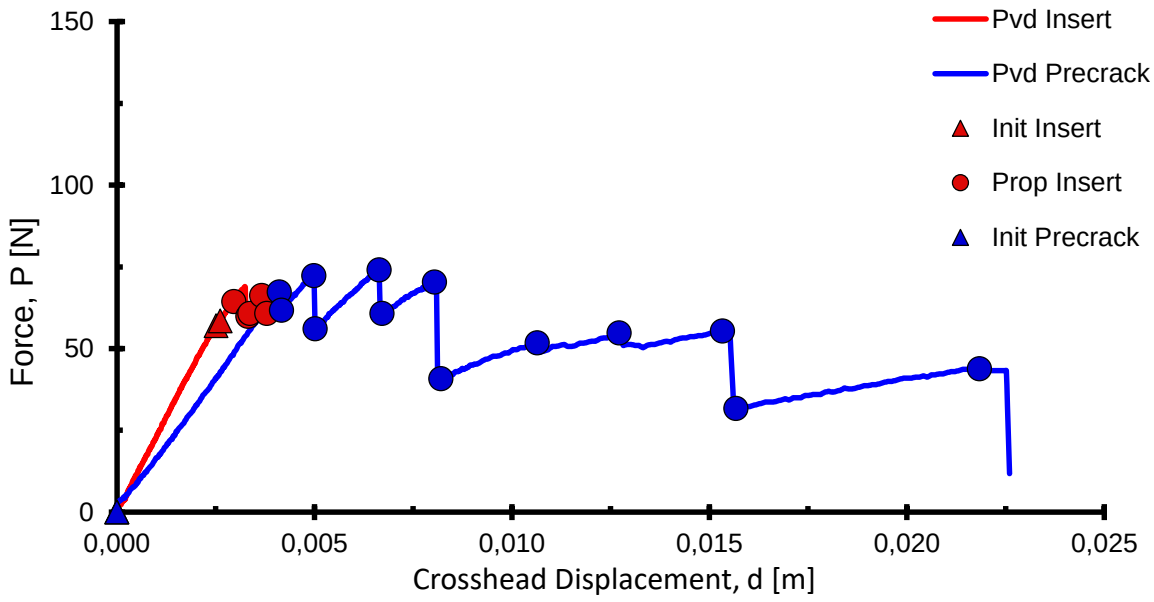

Figure 38. Load-displacement curve for PI transversal strips specimen 1

The R-curves for the four specimens tested are shown in figure 39:

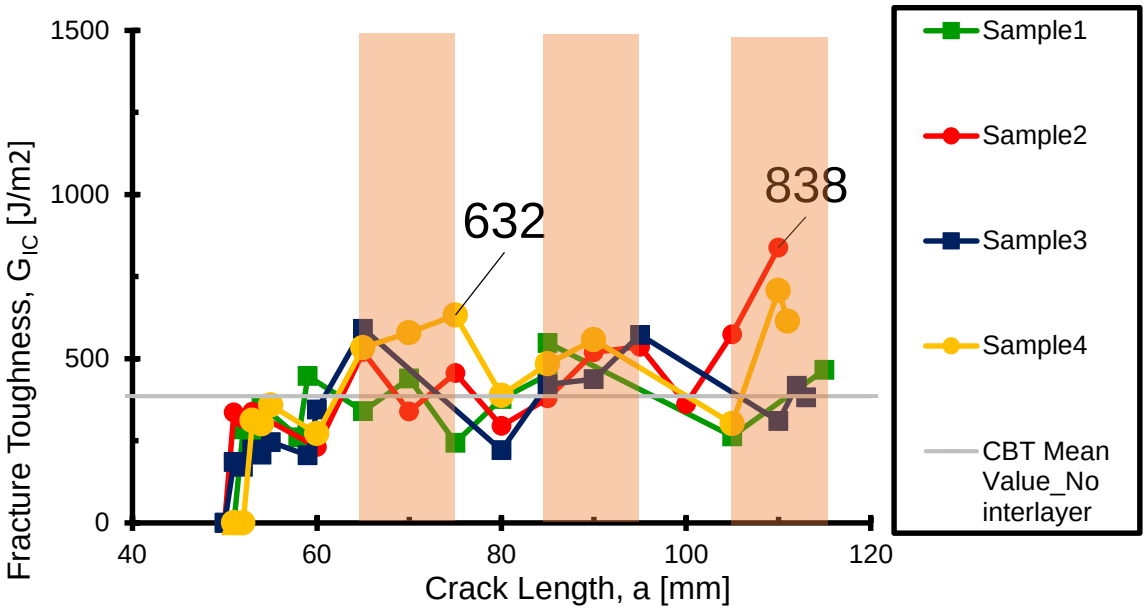

Figure 39. R-curves for PI transversal strips

In this chart, the pink rectangular zones are the zones in which the PI strips were placed. The R-curves show that the fracture toughness is increased in the zones with the transversal strips; the maximum value registered with transversal strips is higher than the maximum one found for longitudinal strips (838 J/m^2 against 752 J/m^2). Figure 40 shows a microscopy of specimen 1:

Figure 40. Microscopy for PI transversal strips specimen 1

The fracture surface appears smooth and without fibers that are peeled away: the fracture was cohesive, the same as the specimens without an interlayer.

5.4.3. PI mesh

Four specimens were produced with the PI mesh, but one got broken during the cutting process; for this reason, only three specimens were available for the testing and the data analysis.

The fracture mechanism, as expected for the presence of transversal strips, was observed to be irregular. For this reason, the mean value is not considered representative of the overall fracture toughness. Load-displacement curve is shown for specimen 2 in figure 41; the R-curves are visible in figure 42:

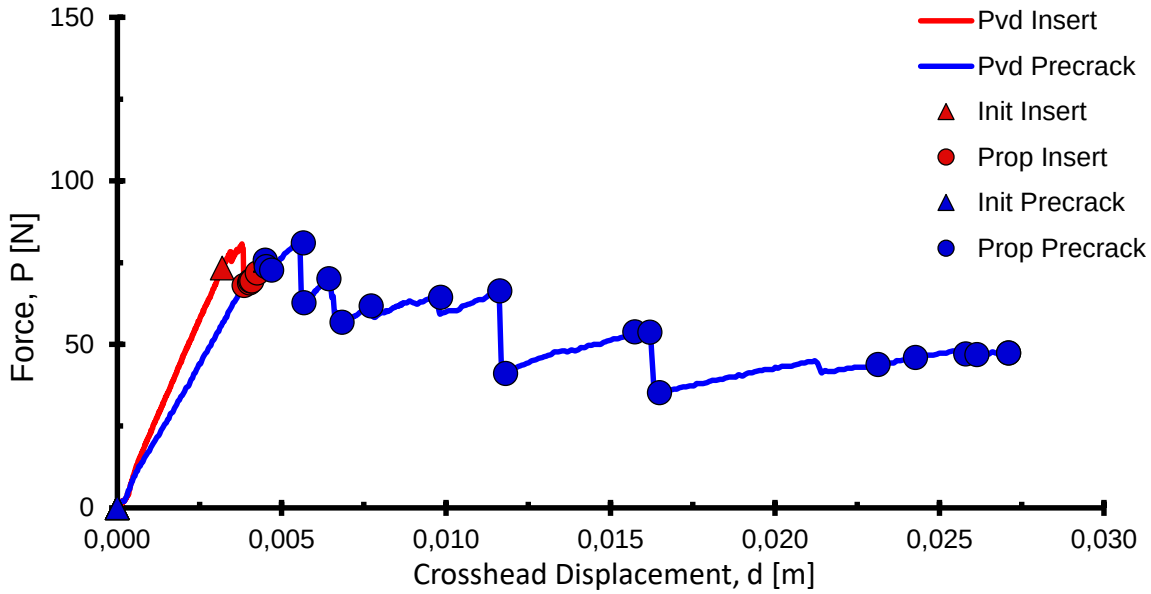

Figure 41. Load-displacement curve for PI mesh specimen 2

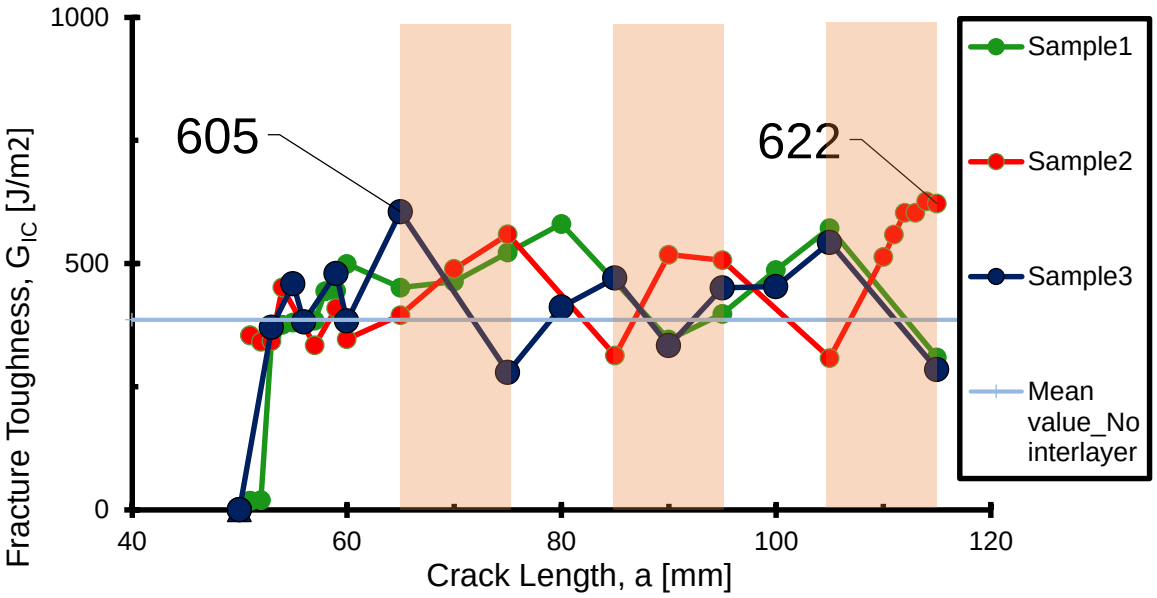

Figure 42. R-curves for PI mesh specimens

From figure 41, the 'saw teeth' characteristic of the stick-slip behavior are visible.

Figure 42 shows that the fracture toughness is increased where the transversal strips are; this effect is particularly visible in specimen 2. Even though the transversal strips improves the resistance to fracture, their effect is mitigated by the presence of longitudinal strips; in fact, the maximum value of G_{IC} is 622 J/m^2, more than 200 J/m^2 lower than the maximum value for transversal strips (838 J/m^2).

For these considerations, the mesh configuration is less effective than the transversal strips.

5.5. Polyethylene Terephthalate (PET)

5.5.1. PET longitudinal strips

The crack propagates in a very stable way. There are no 'jumps' and the crack length can be determined at every point of the test. Because of this great stability, the mean

value is calculated and it represents the fracture toughness faithfully. The stable growth of the crack is visible in figure 43, where specimen 3 is taken as example:

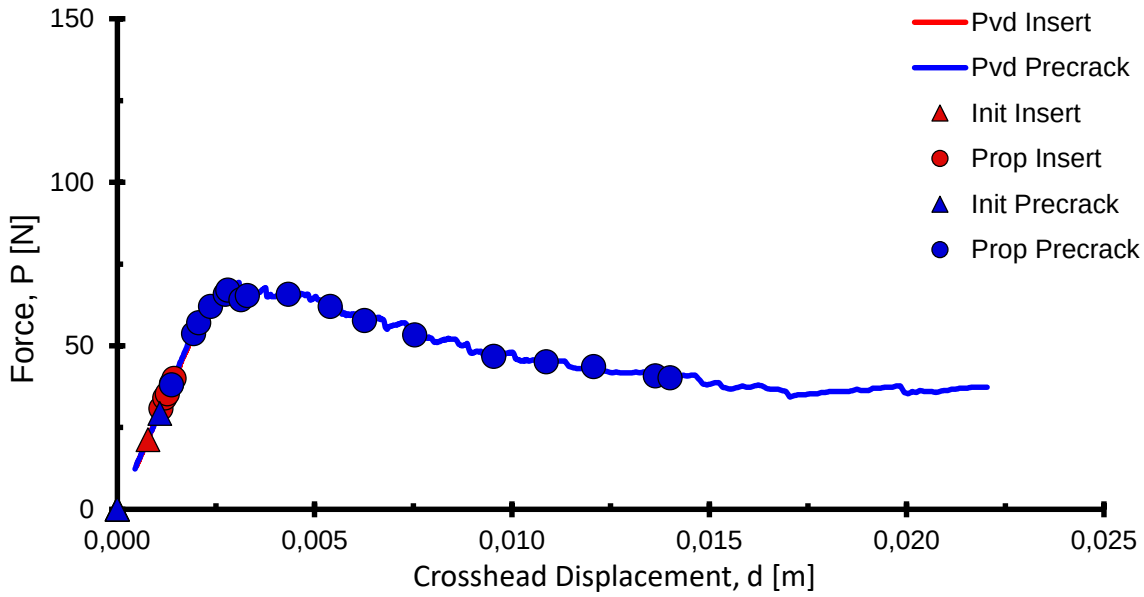

Figure 43. Load-displacement curve for PET longitudinal strips specimen 3

As well as the load-displacement curves, also the R-curves are regular:

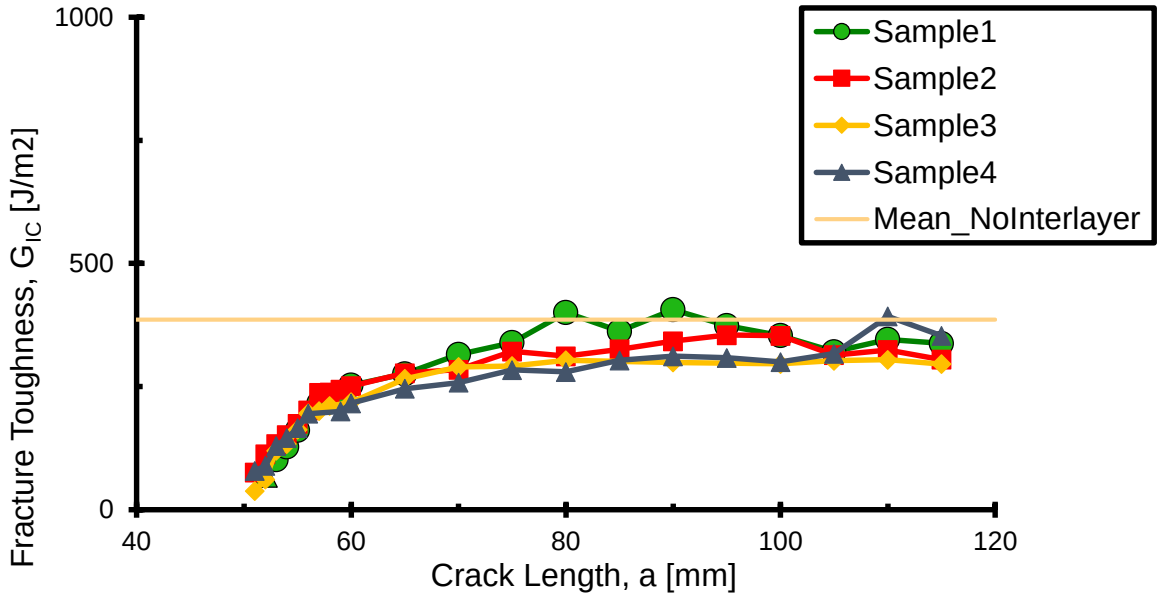

Figure 44. R-curves for PET longitudinal strips

Beside the fact that the curves are almost flat, it is evident how the values of the fracture toughness are lower than the mean value for the specimens without the thermoplastic interlayer (except for two points in specimen 1). This unsatisfying result is represented in figure 45:

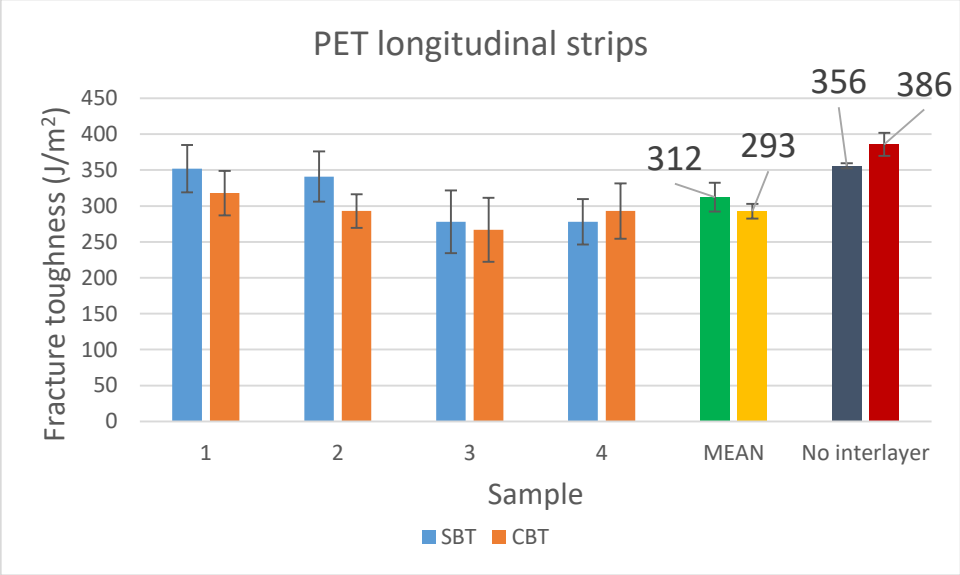

Figure 45. Pet longitudinal strips mean values

Comparing the CBT values, the mean value for the specimens with PET longitudinal strips is about 100 J/m^2 lower than the mean value for the specimens without thermoplastic. This result is disappointing since it means that the interlayer weakens the composite instead of making it tougher. It is believed that this is due to the fact that the PET provides a preferential path for the crack to grow since this thermoplastic is more brittle than the composite.

5.5.2. *PET transversal strips*

The PET transversal strips were observed to have an effect on the mechanism of propagation: the growth was unsteady, with the storage of energy followed by the crack's 'jumps'.

Specimen 1 was taken as example in figure 46, where its load-displacement curve is shown.

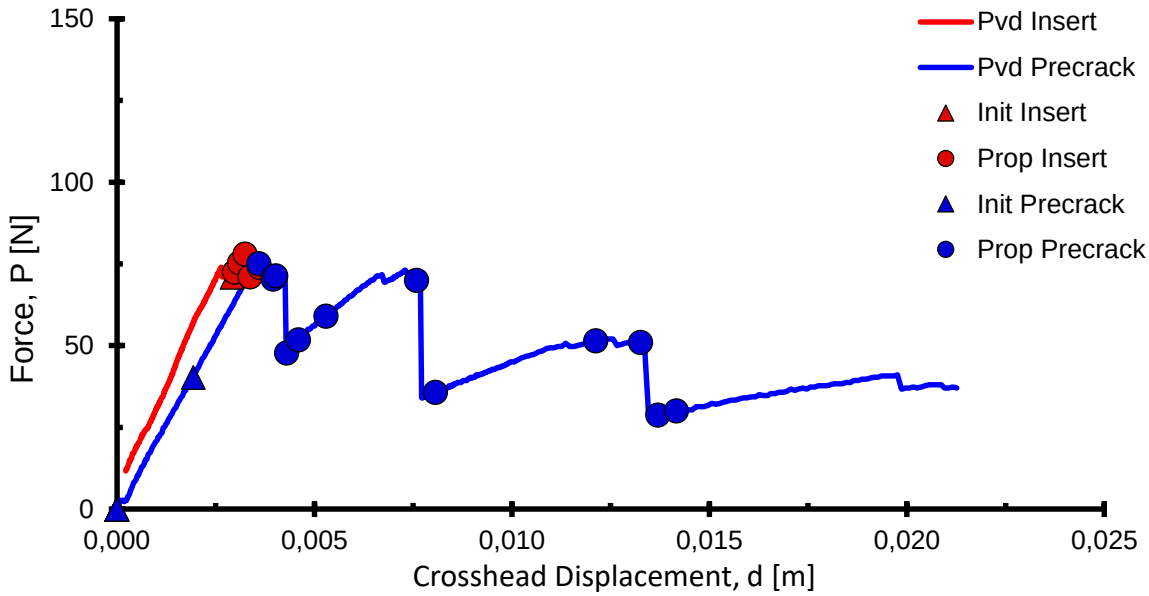

Figure 46. Load-displacement curve for PET transversal strips specimen 1

This behavior leads to non-flat R-curves, shown in figure 47:

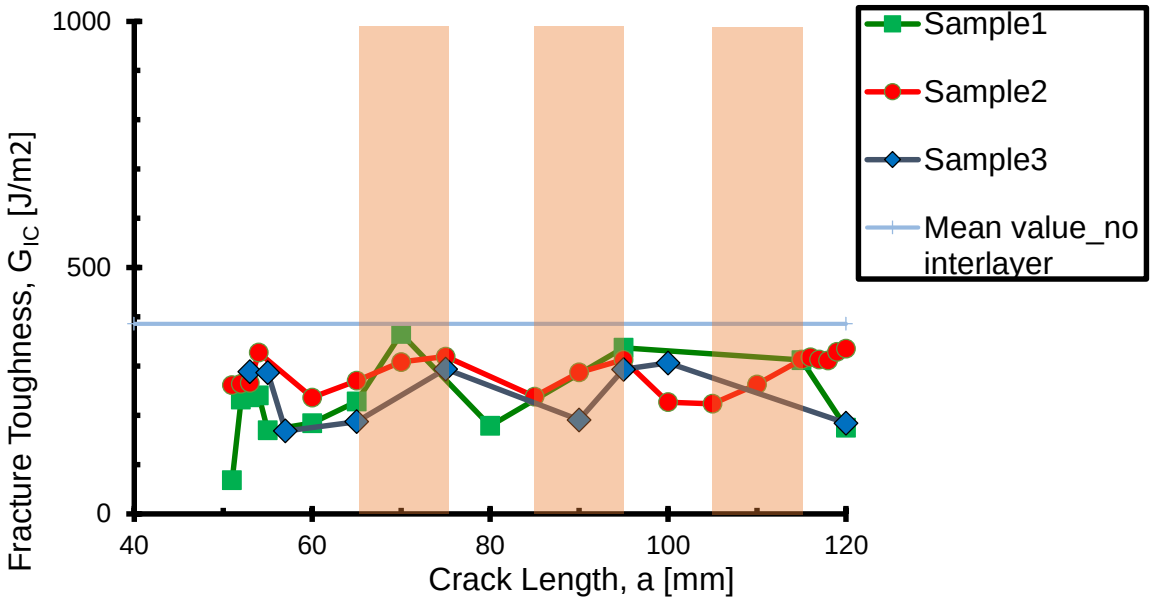

Figure 47. R-curves for PET transversal strips

Analyzing the results, it is observed that the transversal strips have a negative effect on the fracture toughness: values of G_{IC} are lower than the mean value for the specimens without thermoplastic during the entire test. As already found with the PET longitudinal strips, this material has a weakening effect on the CFRP.

5.5.3. PET mesh

Three specimens were tested with the PET mesh. As well as in the other samples with transversal strips, the propagation of the crack was observed to be unstable and the load-displacement curves showed the characteristic ‘saw teeth’; since the fluctuation of the values is high, the mean value was not calculated.

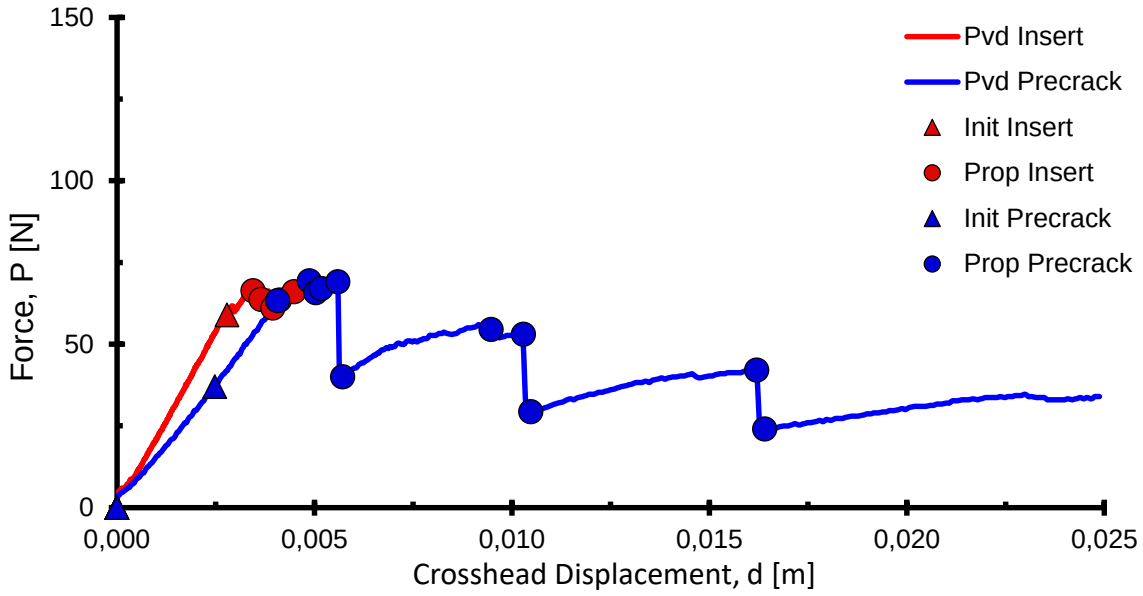

Figure 48. Load-displacement curve for PET mesh specimen 3

The unsteady propagation of the crack causes high fluctuations of G_{IC} values; R-curves are displayed in figure 49.

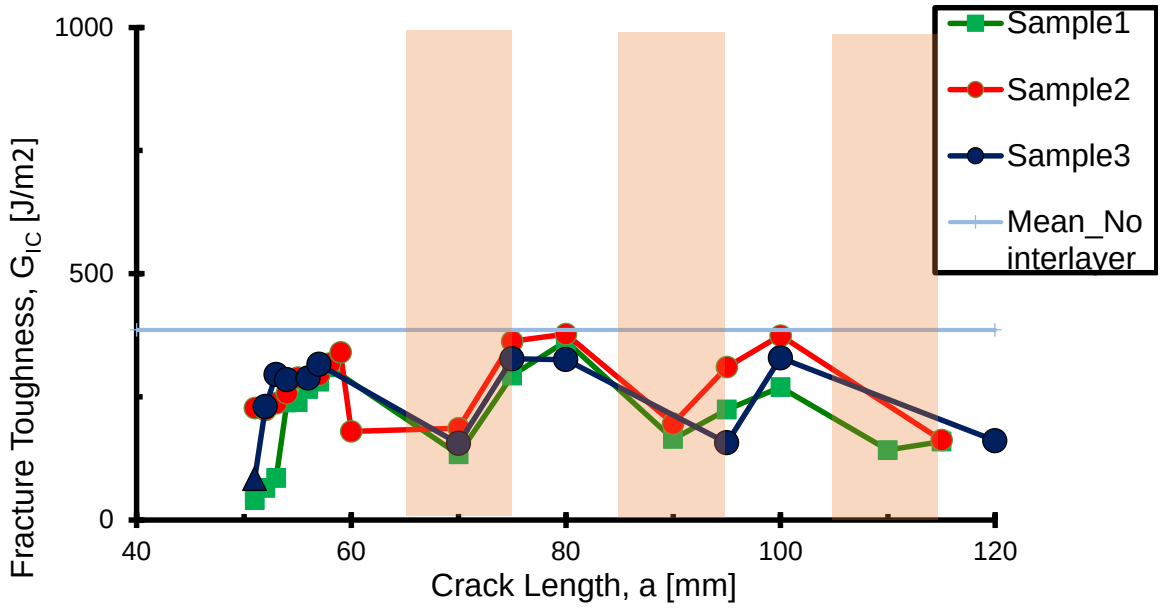

Figure 49. R-curves for PET mesh specimens

From the figure above, the weakening effect of the thermoplastic is visible: in the zones with the PET transversal strips, the fracture toughness drops dramatically. In the zones with just the longitudinal strips, the toughness is comparable to the toughness of the specimens without interlayers.

5.6. Polyetherimide (PEI)

5.6.1. PEI longitudinal strips

In the case of longitudinal strips, the crack propagation is observed to be less regular in comparison with the specimens with the same configuration but different material. In figure 50, it is evident how the crack propagation is irregular, especially in the highlighted sections.

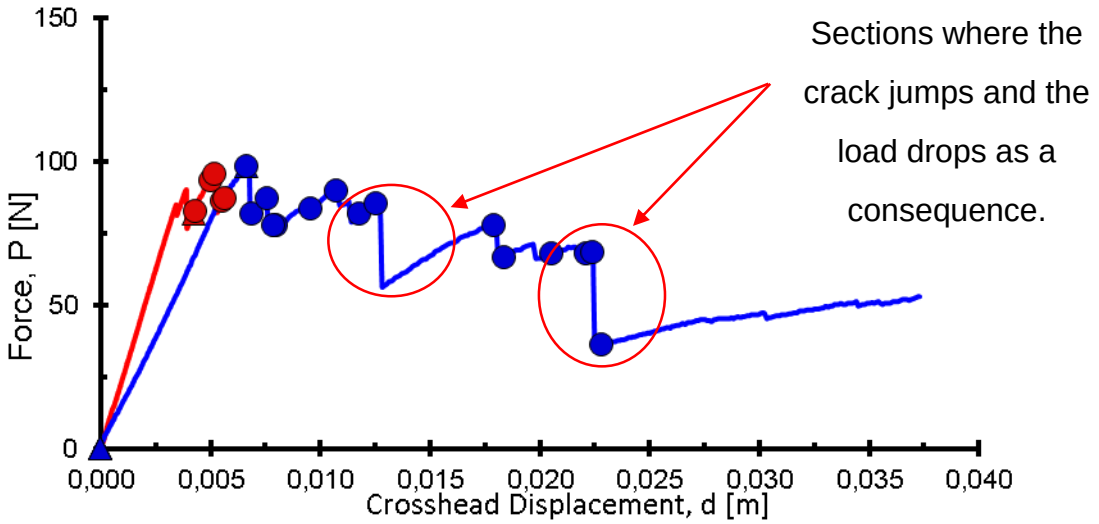

Figure 50: Load-displacement curve, specimen 4 with longitudinal strips

This behavior leads to higher fluctuations of the values of fracture toughness as shown in figure 51.

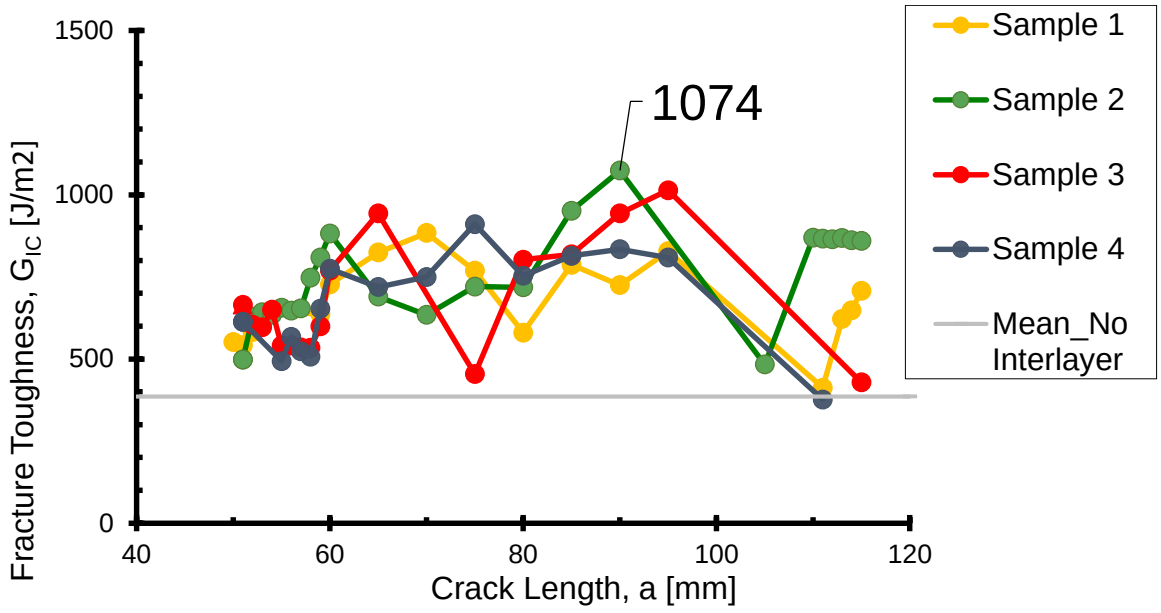

Figure 51. R-curves for PEI longitudinal strips

In the highlighted zones of figure 50, the thermoplastic manages to increase the toughness and therefore the load increases; once the load reaches the critical value, the crack propagates instantly and the load drops until the crack reaches the next point of arrest.

Although the fluctuations are higher than the ones for the specimen without thermoplastic, the mean value calculated throughout the crack length is still considered representative for the fracture toughness and results are shown in figure 52.

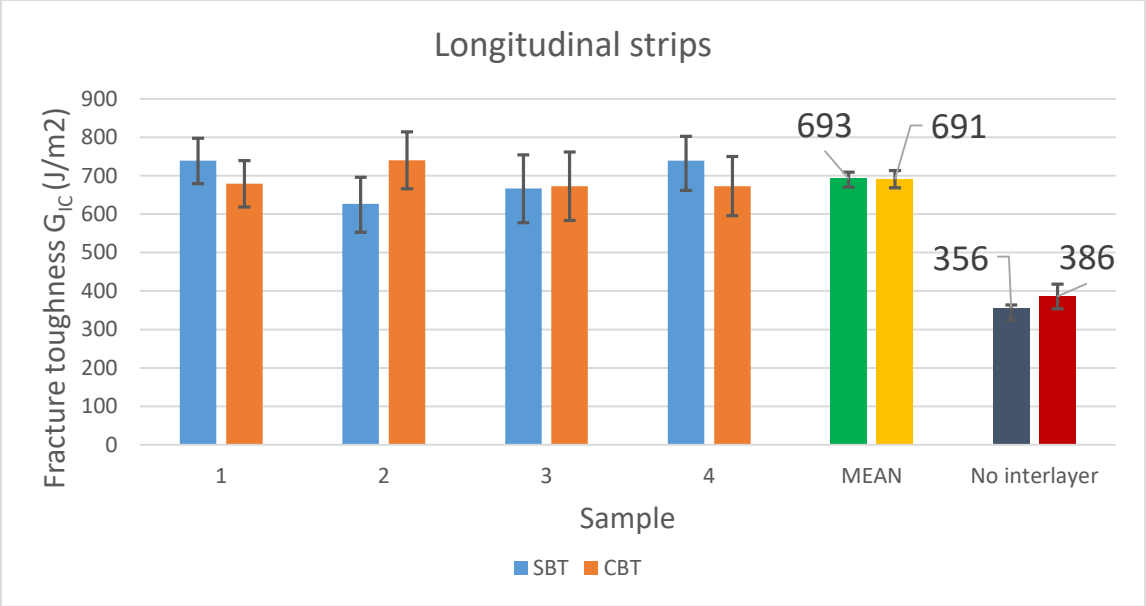

Figure 52: Fracture toughness for specimens with PEI longitudinal strips

The fracture toughness is increased up to 305 J/m^2 (CBT value) over the control. The longitudinal thermoplastic strips have effect both in the crack propagation mechanism and in the toughening of the composite.

The fracture surface shows that the crack propagation occurred by delamination. 0° fibers can be easily peeled away since secondary cracks have grown in between the 0° and 90° fibers in each specimen. Figure 54 shows this mechanism in specimen 1.

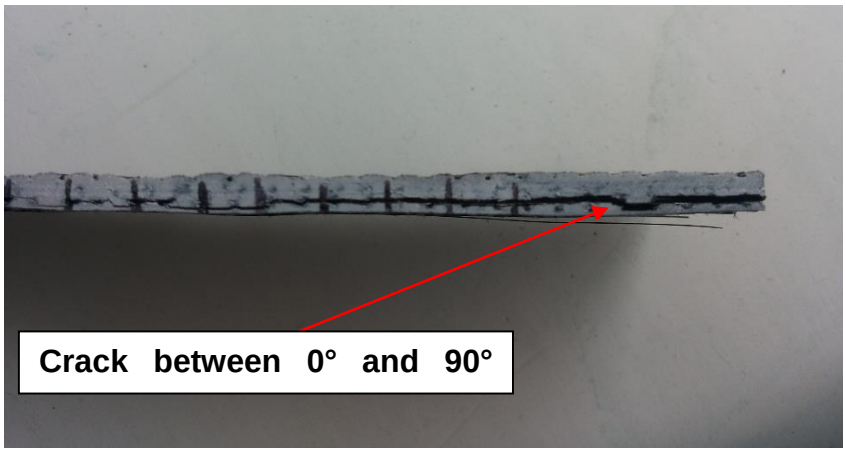

Figure 53. Lateral view of the fibers

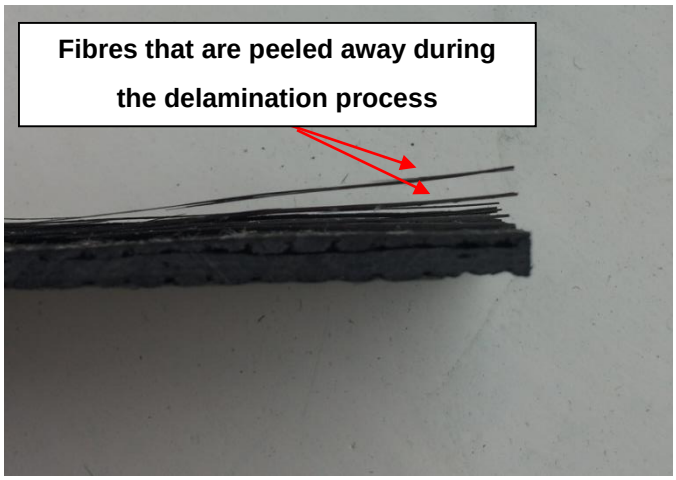

Figure 54: Detail on the fibers

5.6.2. PEI transversal strips

During the testing of specimens with transversal PEI strips, the crack was observed to grow with stick-slip behavior. This mechanism leads to very high fluctuations of G_{IC} values, therefore the mean value of fracture toughness evaluated throughout the crack length ceases to be representative of the real fracture toughness.

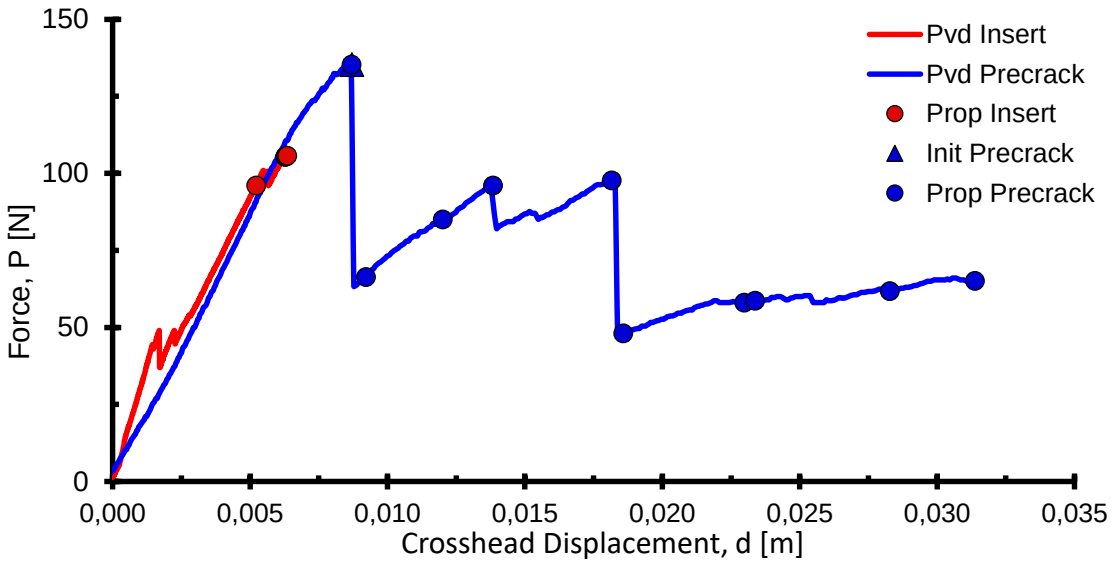

Figure 55: Load-displacement curve for transversal strips specimen 3

Figure 55 shows the stick-slip behavior; the maximum load is 135 N, which is higher than the maximum load for the specimen without interlayer, 71 N.

Figure 56 shows the trend of the fracture toughness against the crack length.

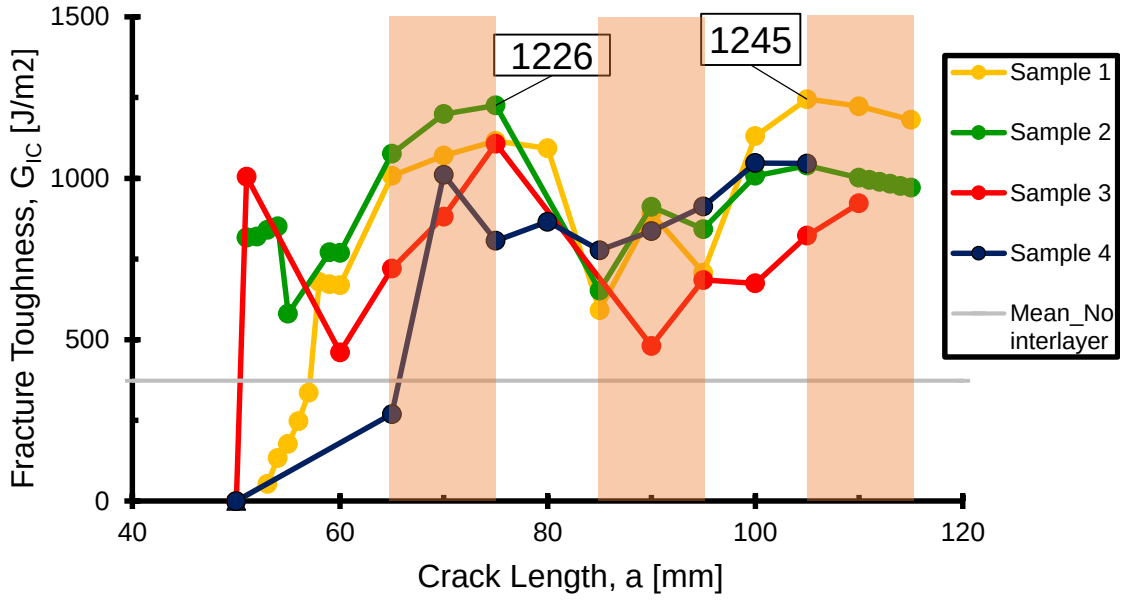

Figure 56. R-curves for transversal strips

The effect of the strips is evident: the fracture toughness is dramatically increased where the strips are. The thermoplastic acts as crack stopper and it is capable of increasing the load required for the crack propagation. The G_{IC} values are higher than the ones obtained with longitudinal strips, in fact for transversal strips the fracture toughness reaches the values of 1226 J/m^2 (specimen 2) and 1245 J/m^2 (specimen 1) while with longitudinal strips the highest value of fracture toughness was 1074 J/m^2. The fracture mechanism is, as with longitudinal strips, delamination. The secondary crack starts growing as soon as it encounters the thermoplastic strip as shown in figure 57. Since the toughness of PEI is extremely high, the fracture cannot propagate as neither adhesive nor cohesive crack; therefore it changes plane growing in between the 0°/90° layers.

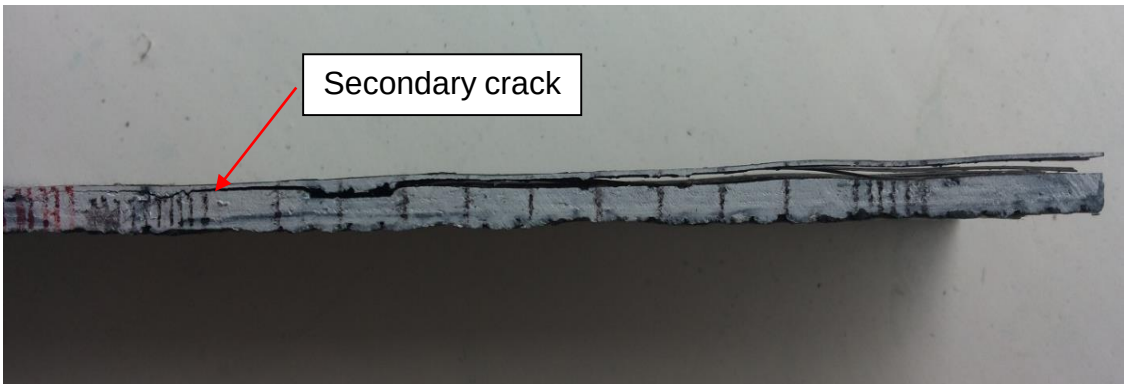

Figure 57. Delamination in transversal strips specimens

5.6.3. PEI mesh

The crack propagation occurred with stick-slip behavior. The fluctuations of G_{IC} values are high and therefore, as with transversal strips, the mean value is not calculated since the standard deviation would be too high to consider it reliable.

Figure 58 shows the stick-slip behavior for specimen 3.

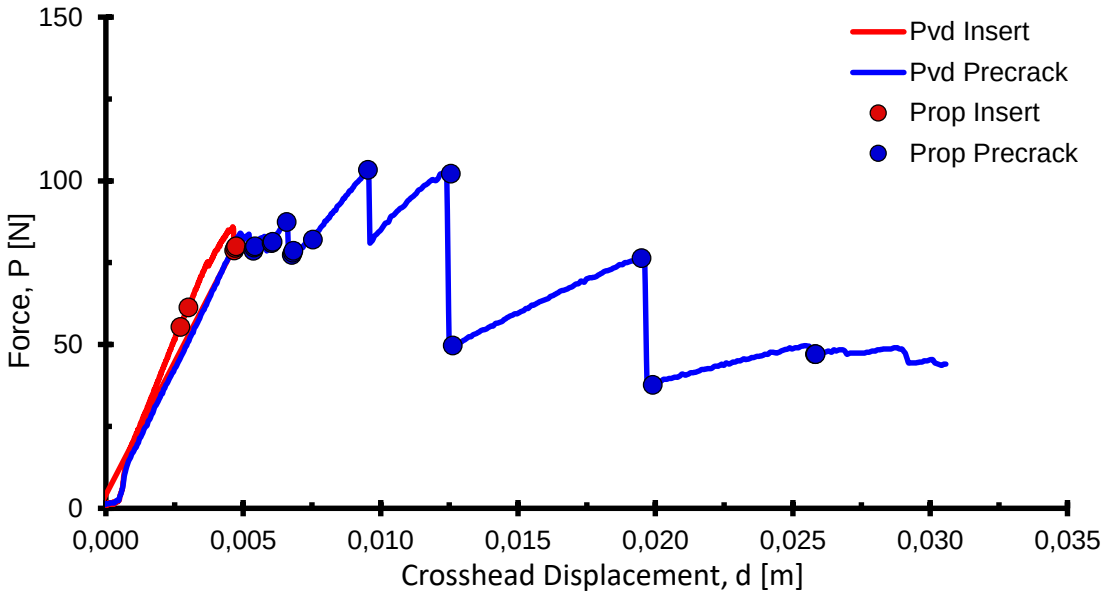

Figure 58: Load-displacement curve for PEI mesh specimen 3.

The R-curves for specimens with thermoplastic mesh are shown in figure 59.

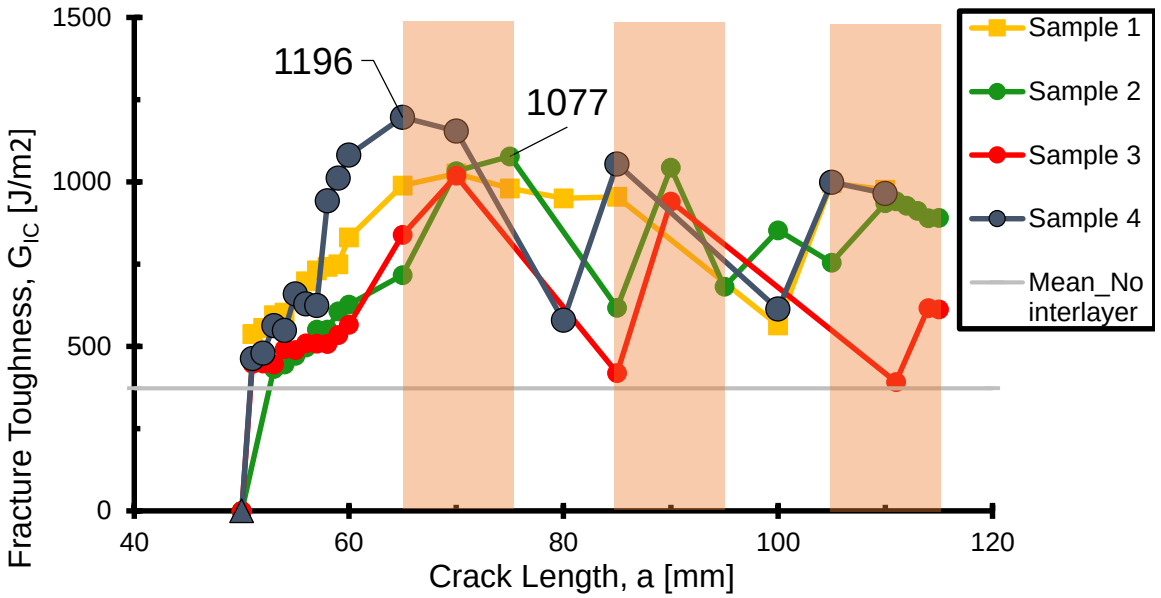

Figure 59: R-curves for specimens with PEI mesh

Since both longitudinal and transversal strips increased the fracture toughness, the mesh was expected to be the most effective geometry. This expectation is refuted by the results: only for specimen 4 the toughness exceeds 1100 J/m^2 meaning that the toughening effect of the transversal strips is reduced by the simultaneous presence of longitudinal strips. The effect of the transversal strips is still visible in the R-curve since the toughness is increased in the zones with transversal PEI.

In none of the specimens there is evidence of a secondary crack as it was with longitudinal and transversals strips. The mechanism of delamination is evident in specimens 1 (figure 61) and 4, less visible in specimen 2 and 3 (figure 60).

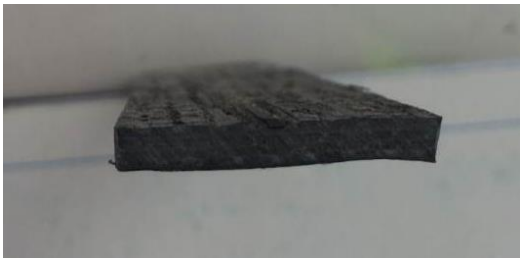

Figure 60: Specimen 3, no visible delamination.

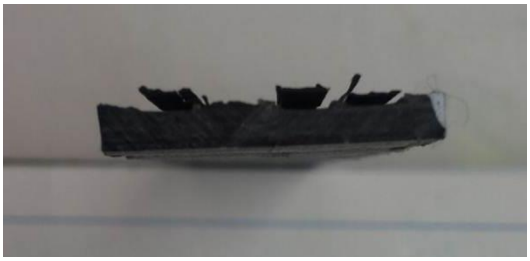

Figure 61: Specimen 1, delamination visible.

5.7. Polymethyl methacrylate (PMMA)

PMMA was the last material tested. The first two plates with longitudinal and transversal strips were produced with the same curing process. Since the results for those specimens were less promising than the results for PEI and there was only one curing process available because of lack of resin and time, it was decided to produce a plate with PEI strips in between different layers of fibers instead of the plate with the PMMA mesh. The results for PEI strips in multiple layers are shown in chapter 5.8.

5.7.1. Longitudinal strips

The crack propagation was observed to be regular, as shown in figure 62:

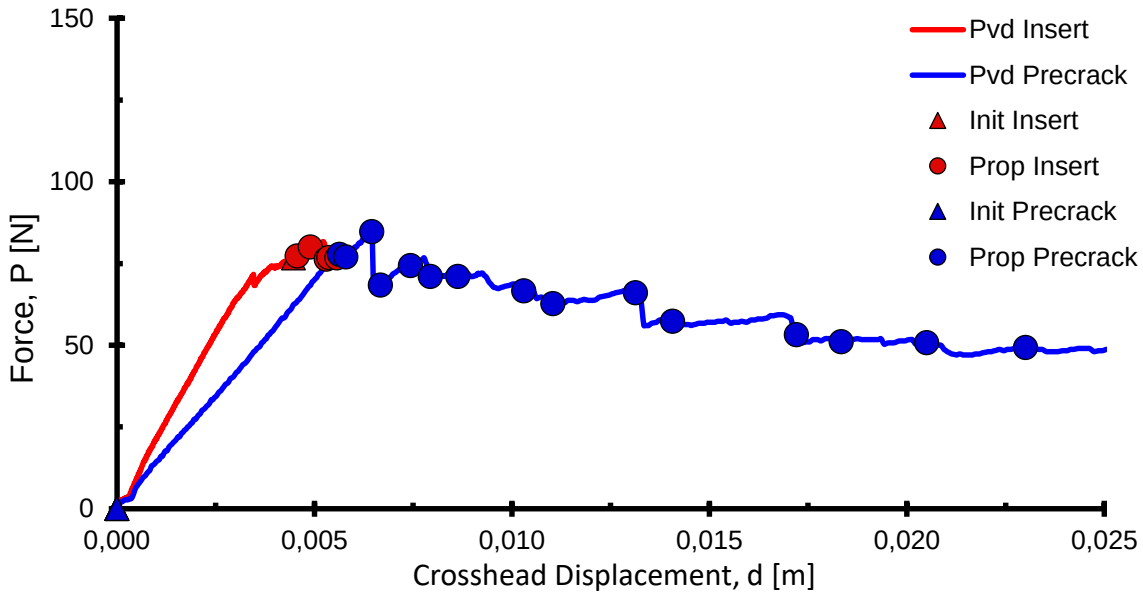

Figure 62. Load-displacement curve for PMMA longitudinal strips specimen 1

As usual, the stability of the crack growth leads to nearly flat R-curves, that are visible in figure 63.

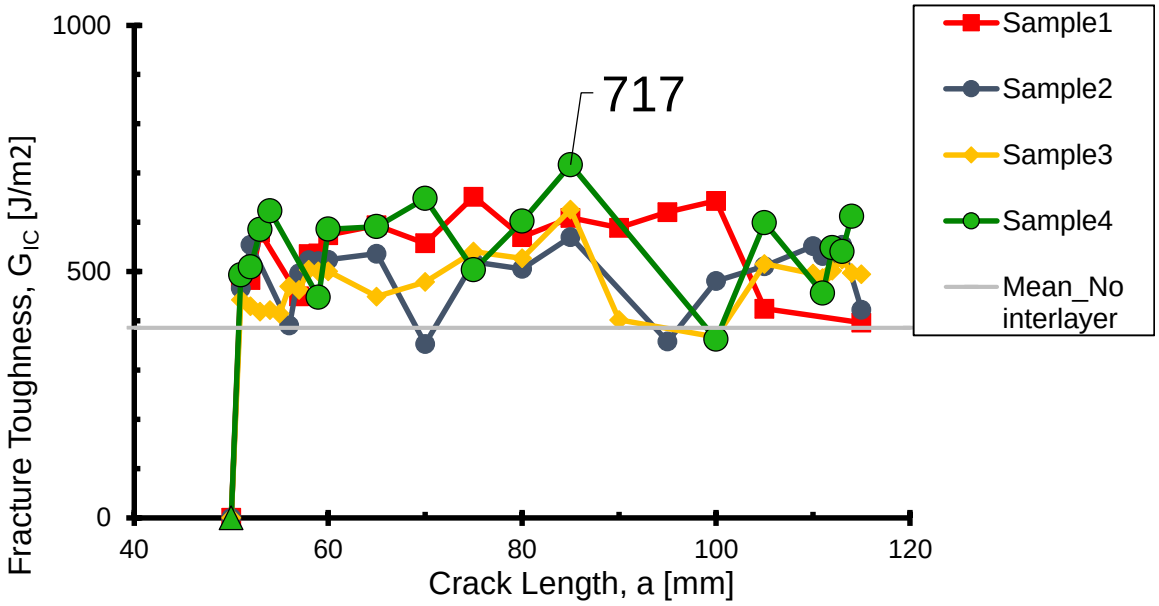

Figure 63. R-curves for PMMA longitudinal strips

Figure 64 shows that the fracture toughness is increased throughout the specimens: since the fluctuation of G_{IC} values is low, the mean value was calculated and it represents the overall fracture toughness.

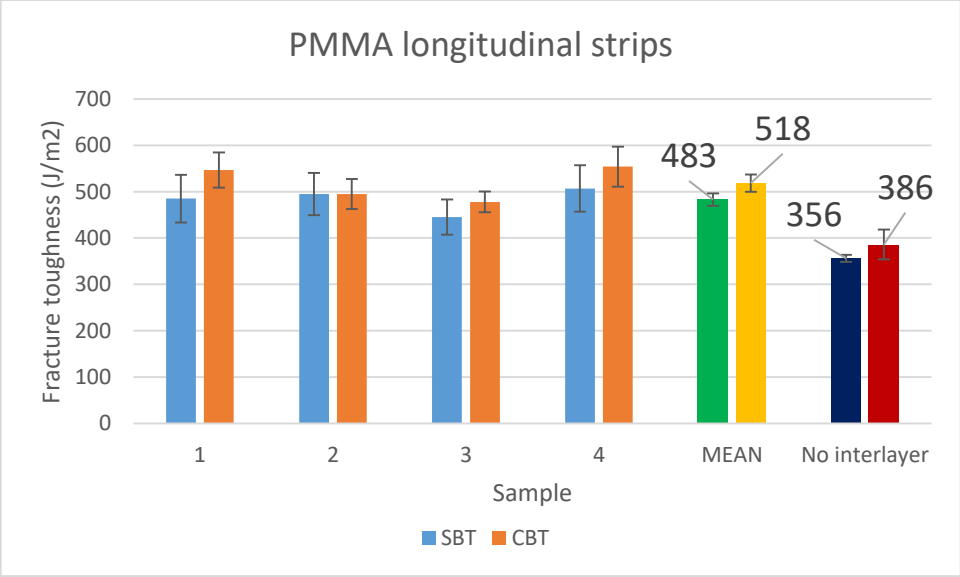

Figure 64. Fracture toughness for specimens with PMMA longitudinal strips

The fracture toughness is increased by 132 J/m^2 up to 518 J/m^2. This result is comparable with the value obtained with PI longitudinal strips (498 J/m^2), but it is lower than the PEI longitudinal strips' value (691 J/m^2).

5.7.2. PMMA transversal strips

The propagation of the crack, as it was found in every other specimen with transversal strips, was observed to be irregular with a stick-slip behavior. Figure 65 represents the load-displacement curve for specimen 4:

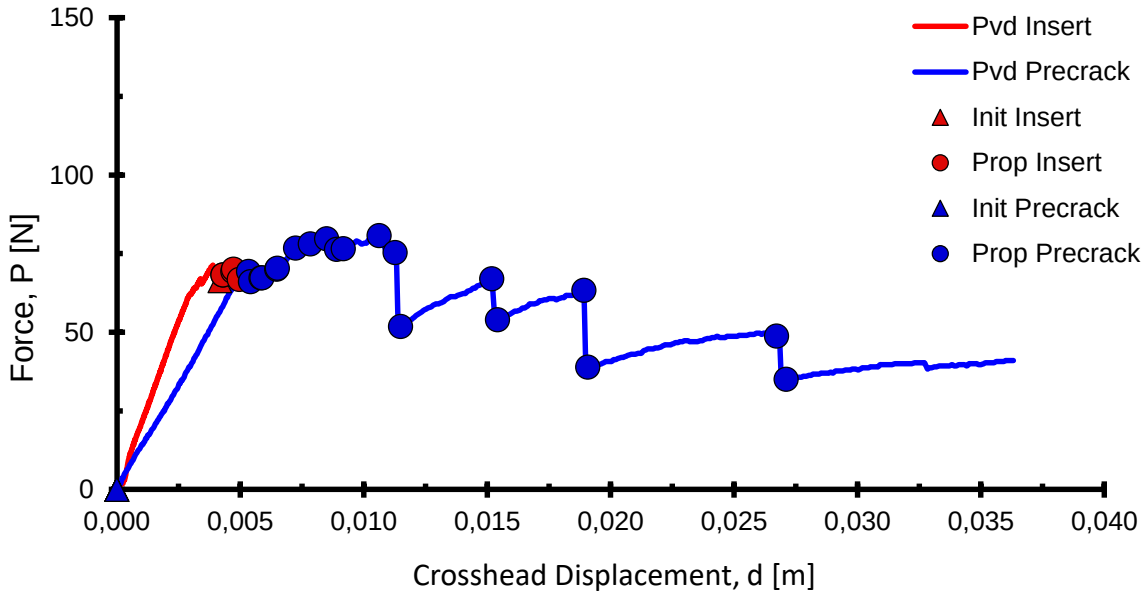

Figure 65. Load-displacement curves for PMMA transversal strips specimen 4

The stick-slip phenomenon causes high fluctuations in the R-curves. This fact is shown in figure 66.

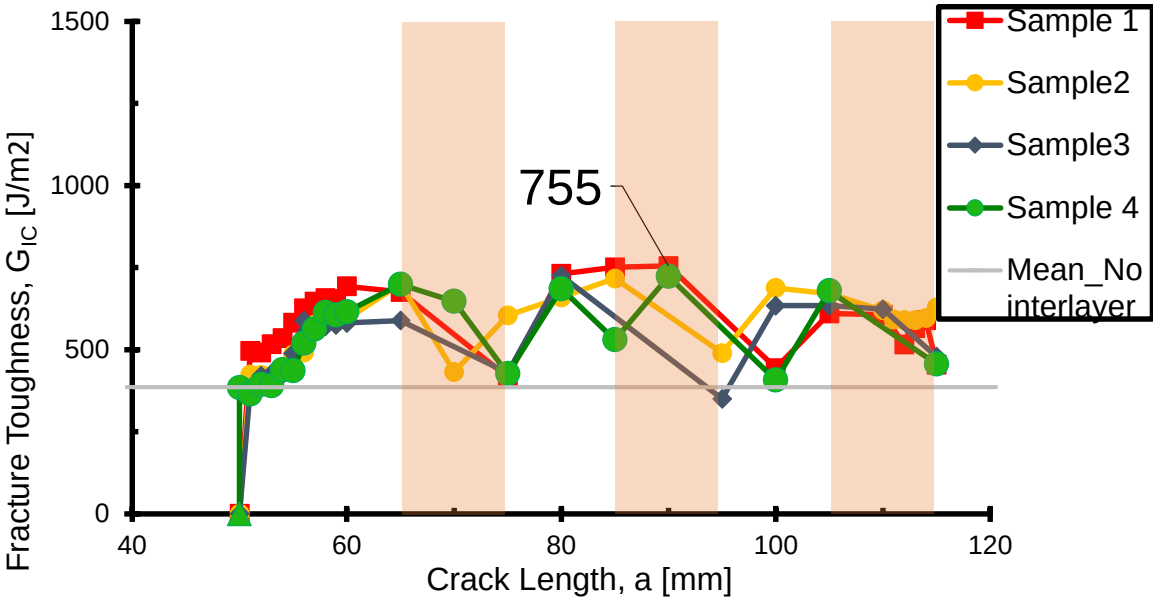

Figure 66. R-curves for PMMA transversal strips specimens

It is evident how the strips increase the toughness. The highest value registered for PMMA transversal strips specimens was 755 J/m^2, confirming that with equal material transversal strips are preferable to longitudinal ones.

The fracture surface shows that the fracture is cohesive. There is no evidence of delamination process, as visible in figure 67.

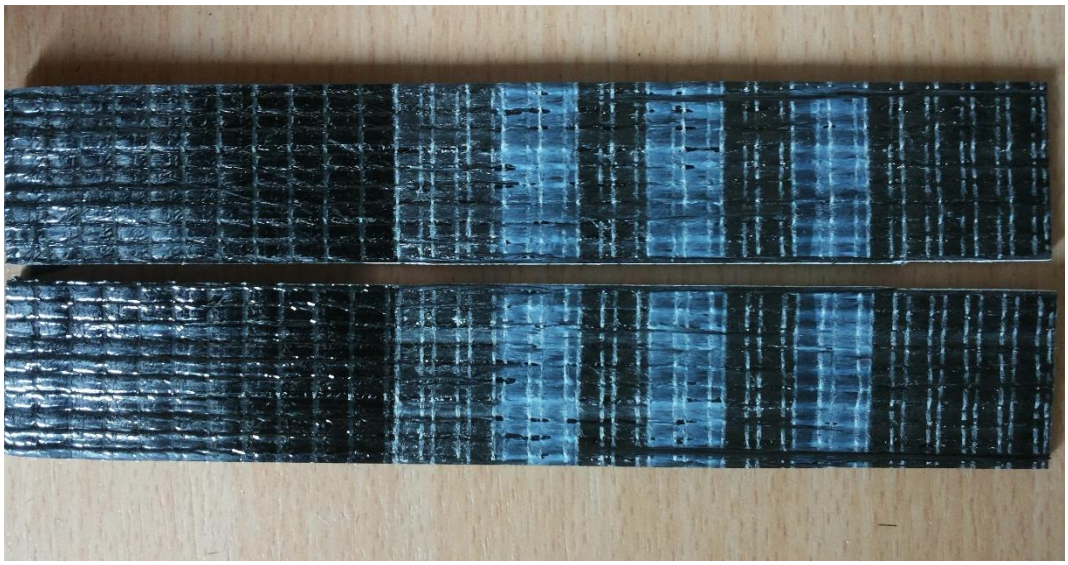

Figure 67. PMMA transversal strips specimen 1

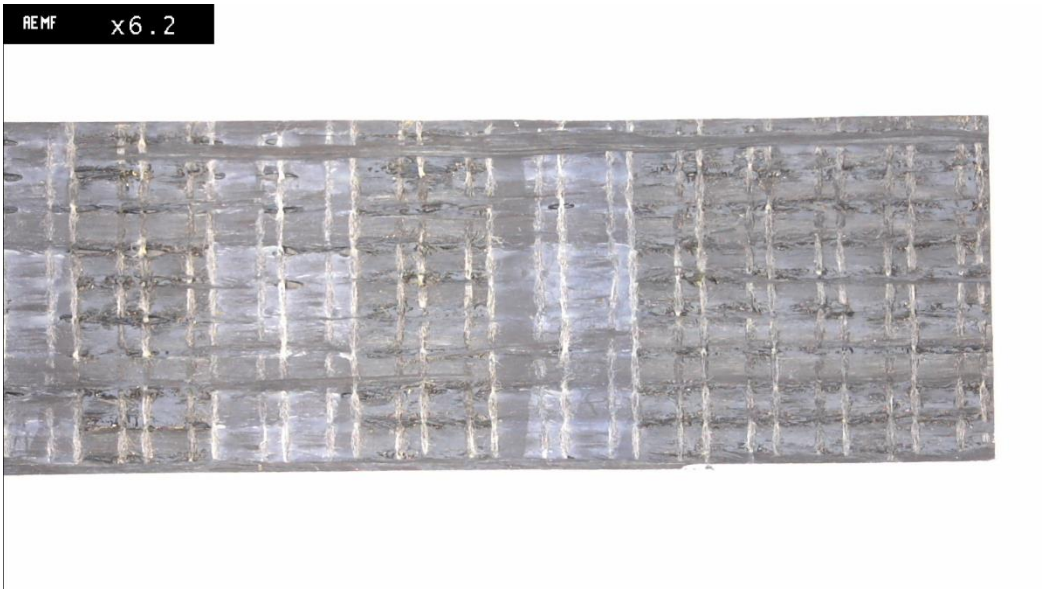

Figure 68. Microscopy for PMMA transversal strips specimen 1

5.8. PEI transversal strips in multiple layers

As already stated in chapter 5.6, PEI transversal strips showed the best results for both the material and the configuration. Figure 69 represents the growth of a secondary crack between 0° and 90° plies. For this reason, it was believed that a thermoplastic interlayer placed in between those plies would have stopped the crack propagation increasing the toughness.

Unfortunately, as already explained in chapter 3.3, the fibers are provided with the 0° and the 90° layers already stitched together. With this issue, it was impossible to insert the interlayer in the desired position.

The secondary cracks in the PEI transversal strips specimens were observed to eventually change the fracture plane, going from the 0°/90° to the 90°/-45° space as shown in figure 69:

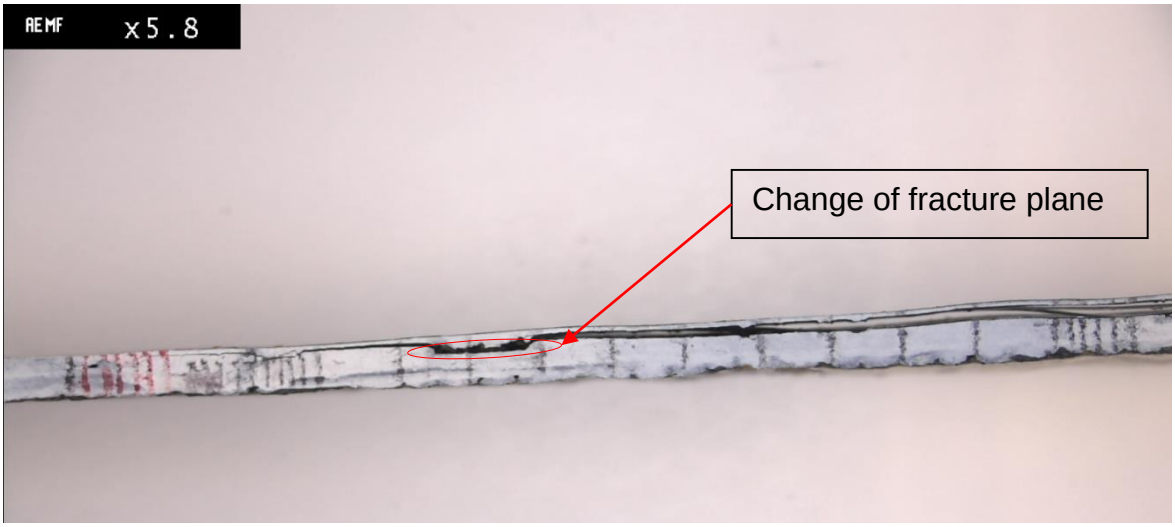

Figure 69. Detail on PEI transversal strips specimen 1

Because of this observation, it was supposed that an interlayer between the 90° and the -45° layers would have increased the fracture toughness.

The plate was produced with the following configuration:

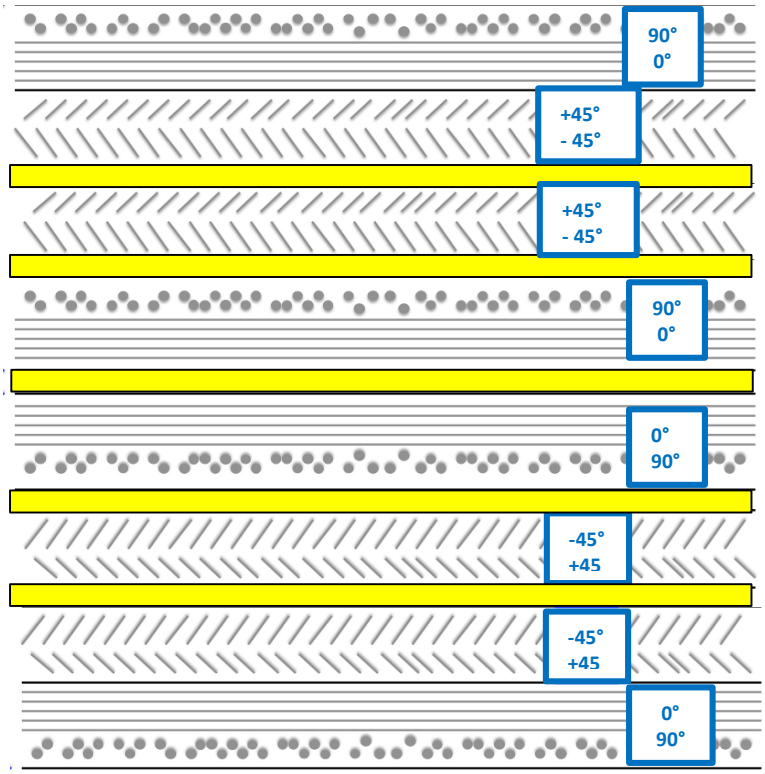

Figure 71. Multiple interlayer configuration

The crack propagation was unstable, as already found with the other configurations with transversal strips. Load-displacement curves for specimen 2 are shown in figure 72:

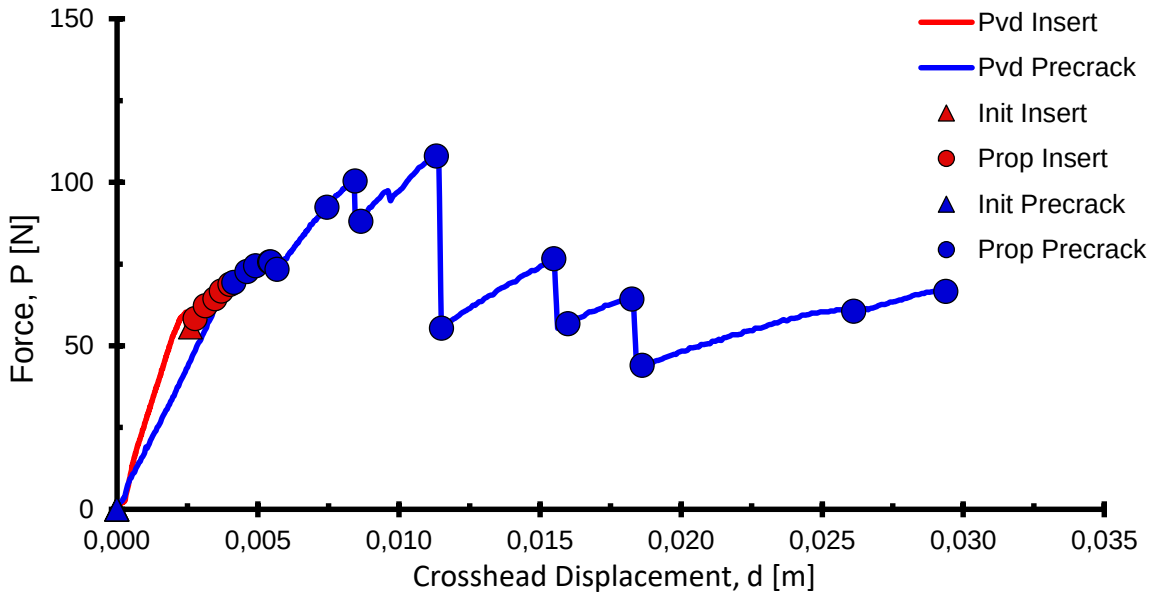

Figure 72. Load-displacement curve for multi-interlayer specimen 2

The R-curves are irregular because of the stick-slip behavior.

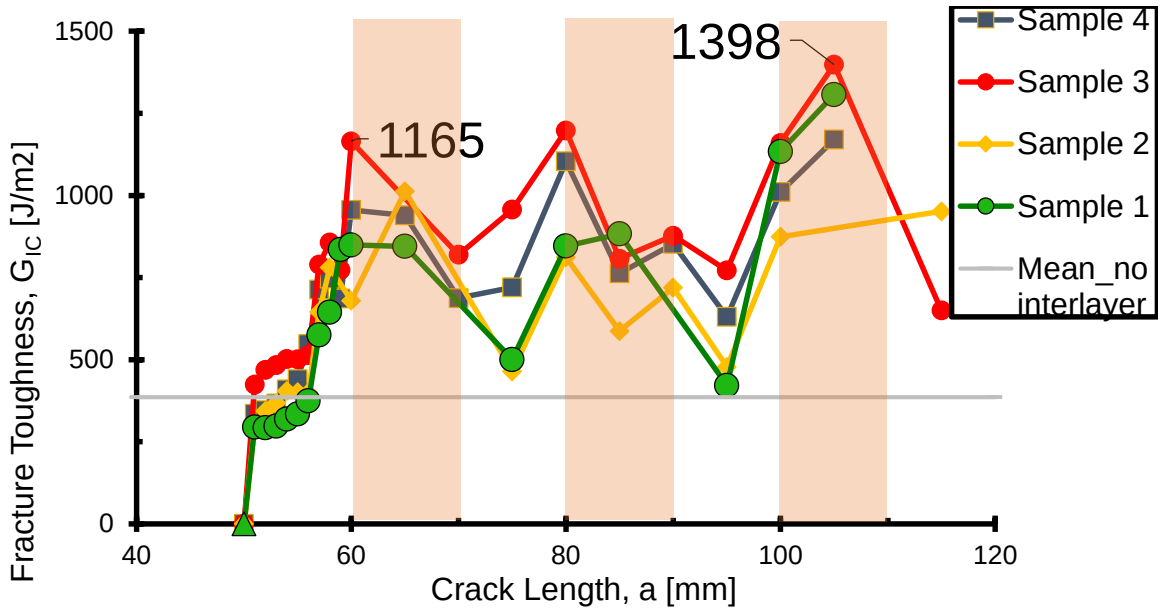

Figure 73. R-curves for multi-interlayer specimens

As expected, the improvement of the multi-interlayer compared to the single interlayer is minimal. Significant results were found only for specimens 1 and 3 in the zone with the last series of strips. This conclusion confirms the fact that the influence of a thermoplastic interlayer between the 90° and -45° is negligible since the secondary crack does not grow in that space. Observation with the optical microscope underlined the delamination process occurring in the specimens as shown in figure 74.

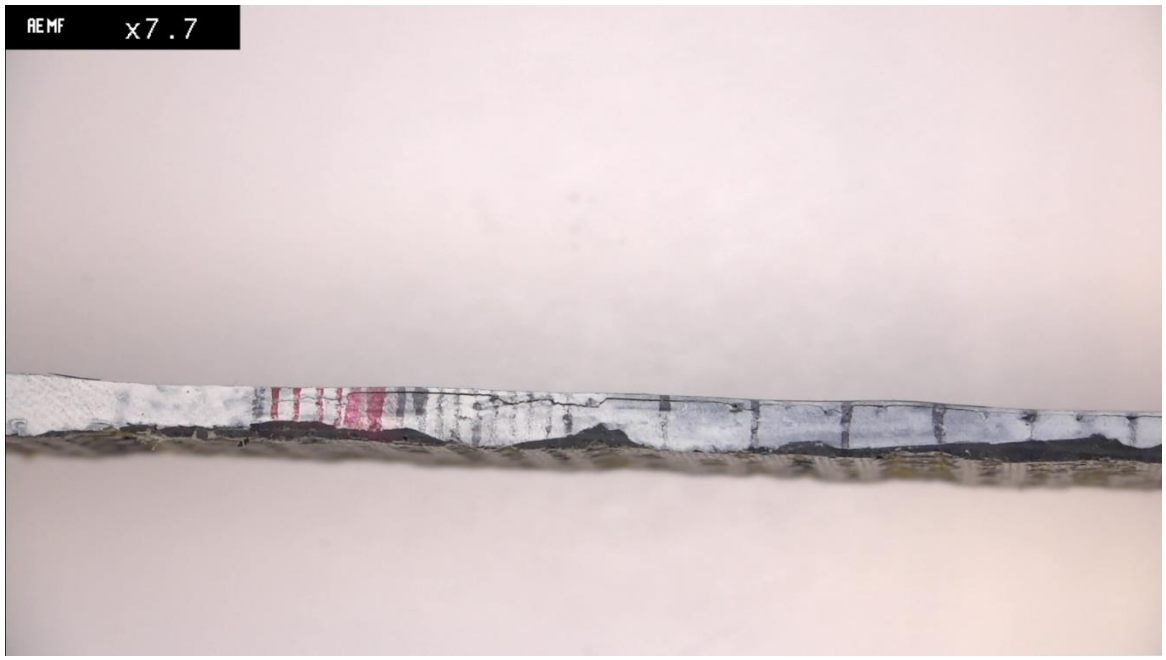

Figure 74. PEI multi-interlayer specimen 2

6. Conclusions

6.1. Summary

Different results were found depending on the materials and orientations tested. The fracture toughness of the specimens with thermoplastic interlayers was compared to the toughness of the 'control' specimens which measured 386 J/m^2.

PET was the worst material among the four thermoplastics used: its addition induced the reduction of the fracture toughness with each of the three configuration tested. The longitudinal strips showed a toughness of nearly 100 J/m^2 lower than the one for specimens without thermoplastic. G_{IC} was reduced also for transversal strips and for PET mesh, but the mean value was not calculated because of the high oscillations of the G_{IC} values.

PI and PMMA interlayers showed comparable results. They both increased the fracture toughness up to a mean value of 500 J/m^2 for longitudinal strips. PMMA was more effective with the transversal strips: the fracture toughness was higher than 386 J/m^2 ('control' value) in the entire length of the crack; instead, PI was able to enhance the crack resistance only in the zones with the strips.

PET, PI and PMMA interlayers induced an unstable propagation of the crack in particular with the transversal strips and the mesh configurations, but the fracture was cohesive as in the control specimens.

PEI showed the best results. With longitudinal strips, this thermoplastic increased the toughness up to 691 J/m^2. The fracture toughness of the specimens with transversal strips had peaks over 1000 J/m^2. Transversal strips and mesh configurations caused delamination of the specimens, with secondary cracks growing out of the middle plane.

Multi-interlayer configuration was trialed with PEI transversal strips, but it did not give promising results since the 0°/90° fibers are stitched together and it was not possible to place the thermoplastic between those layers.

It appears that interlayer strips can be used to tailor the fracture toughness of composite components in a particular direction. Components can benefit from a general increase in fracture toughness with a mesh interlayer, or it can be increased specifically in a preferred direction using transversal strips. Some composite components are designed to take a load in a certain direction during their working life. If a crack occurred in this direction, it is vital that its growth is arrested. However, if the same components experiences an unexpected load in a direction perpendicular to what it is designed for, failure may be preferred as it may protect more expensive components connected to it. In this scenario, transversal strips would be beneficial in a direction perpendicular to the normal loading direction.

6.2. Future work

After the work in this project, the following could be carried out as future work:

- The interlayer orientations in this study could be investigated in failure mode II (in plane shear) and mode III (out of plane shear). As the DCB test only examines failure mode I (crack opening), further testing is necessary. This could verify the results of this project in terms of finding the ideal fiber orientation.

- Mesh cut from a single sheet, as opposed to weaving a mesh could be investigated. For this experiment, a woven mesh was used. This resulted in an interlayer thickness of 0.05 mm in some areas, and a thickness of 0.1 mm

where overlap occurred. This issue might lead to a non-uniform distribution of the resin. By having a single sheet mesh cut, as seen in figure 75, there would be more uniform thickness throughout the samples. This could potentially increase fracture toughness to an even greater level.

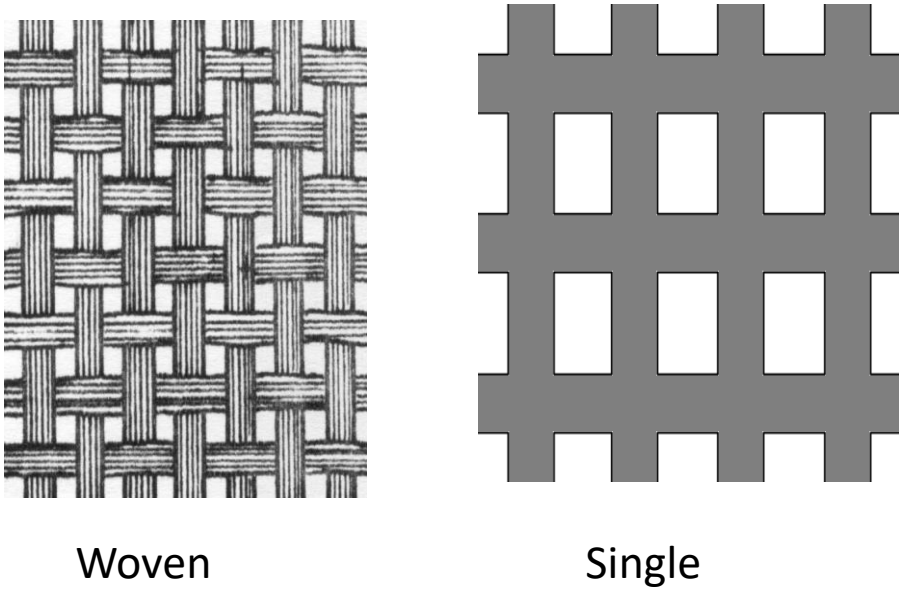

Figure 75: Woven and single sheet mesh types.

- It is believed that having the thermoplastic interlayer between the 0° and 90° fibers would increase the toughness. For this reason, it would be interesting to use fibers where 0° and 90° layers are not stitched together. This additional interlayer would stop the secondary crack propagation forcing the crack to grow inside the thermoplastic, which is tougher than the CFRP.

- Tests at high temperature might be carried out. Since the toughening procedure is based on thermoplastic materials, which have poor thermal properties, it would be interesting to assess the effect of the temperature on the entire system.

- Matsuda et al. showed that fatigue tests gave different results depending on the type of interlayer and the mode of fracture considered [44]. It might be intriguing to investigate the behavior of the thermoplastic interlayers in fatigue tests.

References

[1] D. Kopeliovich, "www.substech.com," 02 June 2012. [Online]. Available: http://www.substech.com/dokuwiki/doku.php?id=classification_of_composites. [Accessed 25 August 2016].

[2] [Online]. Available: http://www.build-on-prince.com/fiber-reinforced-polymers.html#sthash.XgmE57TP.dpbs. [Accessed 25 August 2016].

[3] "Glass Fiber-Reinforced Polymers - A review," *Journal of Reinforced Plastics and Composites,* vol. 33, no. 13, pp. 1258-1275, 2014.

[4] [Online]. Available: http://www.corecomposites.com/products/reinforcements/aramid-hybrids.html. [Accessed 25 August 2016].

[5] A. Ross, "Basalt Fibers: Alternative To Glass?," 8 January 2006. [Online]. Available: http://www.compositesworld.com/articles/basalt-fibers-alternative-to-glass. [Accessed 25 August 2016].

[6] C. Jacques, "Carbon Fiber Composites to More than Double to $36 Billion in 2020," [Online]. Available: http://luxresearchinc.com/news-and-events/press-releases/read/carbon-fiber-composites-more-double-36-billion-2020. [Accessed 25 August 2016].

[7] "Carbon Fiber Reinforced Plastic (CFRP) Market Analysis By Raw Material, By Product, By Application, And Segment Forecasts To 2022," April 2016. [Online]. Available: http://www.grandviewresearch.com/industry-analysis/carbon-fiber-market. [Accessed 25 August 2016].

[8] "boeing.com," [Online]. Available: http://www.boeing.com/commercial/aeromagazine/articles/qtr_4_06/article_04_2.html. [Accessed 25 August 2016].

[9] Jérôme and P. O. R. A., "Composite Materials in the Airbus A380, from History to Future," 2001.

[10] "Challenges in Composites," *Aircraft Technology,* no. 116, pp. 52-57, 2013.

[11] M. Mrazova, "Advanced composite materials of the future in," *INCAS BULLETIN,* vol. 5, no. 3, p. 139 – 150 , 2013.

[12] W. Brostow and H. E. H. Lobland, "Brittleness of materials: implications for composites and a relation," *J Mater Sci,* pp. 242-250, 2010.

[13] L. Jacques, "Computation of Failure Probability: Application to Component Design," in *Brittle Fracture and Damage of Brittle Materials and Composites* , Paris, CNRS (National Centre of Scientific Research), France, 2016, pp. 169-192.

[14] T. Chen, F. A. Mohamed and M. L. Mecartney, "Threshold stress superplastic behavior and dislocation activity in a three-phase alumina–zirconia–mullite composite," *Acta Materialia,* vol. 54, no. 17, p. 4415–4426, 2006.

[15] X. Feng, "Fracture and toughening of soft elastic composite," Iowa State University, Ames, 2016.

[16] B. Hayes and L. Gammon, "Toughening of Fiber Reinforced Composite Materials," in *Microsc Microanal*, Seattle, 2008.

[17] A. Kinloch, R. Mohammed, A. Taylor, S. Sprengers and D. Egan, "The interlaminar toughness of carbon-fibre reinforced plastic composites using 'hybrid-toughened' matrices," *Journal of Materials Science,* vol. 41, no. 15, pp. 5043-5046, 2006.

[18] D. S. Parker and A. Yee, "Factors influencing the mode I interlaminar fracture toughness of a rubber toughened thermoplastic matrix composite," University of Michigan, Ann Arbor, 1989.

[19] J. Kim, C. Baillie, J. Poh and Y.-W. Mai, "Fracture toughness of CFRP with modified epoxy resin matrices," *Composites Science and Technology,* vol. 43, no. 3, pp. 283-297, 1992.

[20] M. Arai, T. Sasaki, S. Hirota, H. Ito, N. Hu and M. Quaresimin, "Mixed modes interlaminar fracture toughness of CFRP toughened with CNF interlayer," Elsevier Science, Nagano, 2013.

[21] H. Faleh, L. Shen and R. Al-Mahaidi, "Fabrication and mechanical characterization of carbon nanotubes-enhanced epoxy," *Advanced Materials Research,* vol. 168, pp. 1102-1106, 2011.

[22] M. Hojo, S. Matsudab, M. Tanakaa, S. Ochiaic and A. Murakamib, "Mode I delamination fatigue properties of interlayer-toughened CF/epoxy laminates," *Composites Science and Technology,* vol. 66, no. 5, pp. 665-675, 2006.

[23] M. Hojoa, T. Andoa, M. Tanakaa, T. Adachia, S. Ochiaib and Y. Endoc, "Modes I and II interlaminar fracture toughness and fatigue delamination of CF/epoxy laminates with self-same epoxy interleaf," *International Journal of Fatigue,* vol. 28, no. 10, p. 1154–1165, 2006.

[24] J. Mohan, "An investigation of composite-to-composite bonding," UCD, Dublin, 2010.

[25] A. A. Griffith, The phenomena of rupture and flow in solids, London: The Royal Society, 1920.

[26] A. J. Brunner, B. R. K. Blackman and P. Davies, "Mode I delamination," in *Fracture Mechanics Testing Methods for Polymers, Adhesives and Composites*, Amsterdam, Elsevier Science, 2001, pp. 277-305.

[27] D. Kopeliovich, "SubsTech," 3 May 2014. [Online]. Available: http://www.substech.com/dokuwiki/doku.php?id=fundamentals_of_adhesive_bonding. [Accessed 25 August 2016].

[28] B. R. K. Blackman and A. J. Kinloch, "Fracture Tests for Structural Adhesive Joints," in *Fracture Mechanics Testing Methods for Polymers, Adhesives and Composites*, Amsterdam, Elsevier Science, 2001.

[29] T. Webb and E. C. Aifantis, "Stick-slip instabilities in fracture," in *Computational Mechanics '95*, Berlin, Springer Berlin Heidelberg, 1995, pp. 1353-1358.

[30] G. R. Irwin, "Analysis of stresses and strains near the end of a crack traversing a plate," *Journal of Applied Mechanics 24,* pp. 361-364, 1957.

[31] G. Williams, "The Fracture Mechanics of Delamination Tests," *The Journal of Strain Analysis for Engineering Design,* pp. 207-214, October 1989.

[32] [Online]. Available: https://www.researchgate.net/figure/291832085_fig11_Figure-8-Crack-resistance-curves-R-curves-for-fracture-of-a-brittle-and-b-ductile. [Accessed 25 August 2016].

[33] E. C. f. Standardization, *ISO 14125:1998: Fibre-reinforced plastic composites: Determination of flexural properties,* Brussels, 2002.

[34] "http://www.datapointlabs.com/," [Online]. Available: http://www.datapointlabs.com/testpaks/3pointbending.htm. [Accessed 25 August 2016].

[35] R. S. Wilson, M. A. Braniff and W. J. T. Millar.Great Britain Patent GB2316036, 1998.

[36] Bombardier. [Online]. Available: http://uk.bombardier.com/en/aerospace/presence-in-country/engineering.html.

[37] 1 October 2011. [Online]. Available: http://www.compositesworld.com/news/saertex-selected-to-supply-material-for-two-bombardier-planes.

[38] [Online]. Available: http://www.multiaxialfabricselcom.com/en/Technology/advantages-of-our-ncf-and-woven-fabric-products.html.

[39] A. v. d. Vegt and L. E. Govaert, Polymeren: van keten tot kunststof, Amsterdam: VSSD, 2005.

[40] R. Akkerman, P. Reed and K. a. W. L. Huang, "omparison of fracture toughness (GIC) values of polyetherimide (PEI) and a carbon-fibre/PEI composite: an experimental and theoretical study," in *Second ESIS TC4 Conference on Fracture of Polymers, Composites and Adhesives*, Les Diablerets, 1999.

[41] B. S. Institution, *BS 7991:2001 Determination of the mode I adhesive fracture energy GIC of structure adhesives using the double cantilever beam (DBC) and tapered double cantilever beam (TDCB) specimens,* London: BSI, 2001.

[42] E. E. Gdoutos, P. M. Schubel and I. M. Daniel, "Determination of critical tearing energy of tyre rubber," Northwester University, Evanston, Illinois, 2014.

[43] A. J. Brunner, B. R. K. Blackman and P. Davies, "A status report on delamination resistance testing of polymer-matrix," *Engineering Fracture Mechanics,* pp. 2779-2794, June 2008.

[44] S. Matsuda, M. Hojo and S. Ochiai, "Mesoscopic Fracture Mechanism of Mode II Delamination Fatigue Crack Propagation in Interlayer-Toughened CFRP," *JSME International Journal Series A,* vol. 40, no. 4, pp. 423-429, 1997.

[45] A. International, *ASTM D5528-13,* West Conshohocken, PA, 2013.

[46] A. International, *Standard Test Methods for Flexural Properties of Unreinforced and Reinforced Plastics and Electrical Insulating Materials,* West Conshohocken, PA, 2015.

[47] [Online]. Available: http://hypertextbook.com/facts/2004/KarenSutherland.shtml. [Accessed 25 August 2016].